Electronic Supplementary Material (ESI) for RSC Advances.

Supplementary Information

Side-by-Side Comparison of Notch- and C83 Binding to γ-Secretase in a Complete Membrane Model at Physiological Temperature

Budheswar Dehury[1,2], Ning Tang[1], Rukmankesh Mehra[1], Tom L. Blundell[2], and Kasper P. Kepp[*1]

[1]*Department of Chemistry, Technical University of Denmark, DK-2800 Kongens Lyngby, Denmark*

[2]*Department of Biochemistry, University of Cambridge, Tennis Court Road, CB2 1GA, UK*

[*] Corresponding author. E-mail: kpj@kemi.dtu.dk. Phone: +045 45252409

Supporting Text: Dynamical stability of γ-secretase-substrate complexes

To evaluate the conformational stabilities of the membrane-embedded γ-secretase-substrate complexes, we computed the backbone RMSD, R_g, and SASA relative to the starting structure of each simulation. The RMSD, R_g, SASA and RMSF of γ-secretase-C83 were obtained from our recently published study of this system.[1] The overall dynamic evolution of each of the three independent trajectories for both γ-secretase-C83 and Notch100 complexes is summarized in **Figure 2A-2B**. Both systems reach stable ensembles after ~200 ns, which is in agreement with our previous simulations of all-atom apo-γ-secretase[2] and C99 bound conformations[3] in homogeneous POPC lipid bilayer systems, and in agreement with the typical time 100-ns scale of the relevant helix-helix orientations.[4] Therefore, we collected statistics for the last 300 ns of the trajectories in all discussions below.

For C83, the average backbone RMSD is 2.79, 3.07 and 3.0 Å for the three independent simulations, whereas for Notch100 it is 3.01, 2.78 and 2.97 Å, i.e. the complexes remained close to the experimental structures 6IYC[5] and 6IDF[6], which have resolutions of 2.6 and 2.7 Å, respectively. Recently, MD simulations by several expert groups have revealed detailed dynamics of this important system. An important MD study on apo-γ-secretase (5FN2) for 1 μs by Hitzenberger and Zacharias[7] reported the Cα-RMSD of the membrane spanning parts remained within ~ 2 Å, which corroborates well with our study. Another insightful all-atom μs-MD study of apo γ-secretase by Aguayo-Ortiz and co-workers[8] displayed backbone RMSD up to 4 Å as compared to starting structure, indicating again the important room temperature dynamics. We analyzed the RMSD for each subunit NCT, PS1, APH1-A, PEN2 and the substrates (**Figure S2−S3**). As expected, the extracellular domain of NCT (NCT-ECD) displayed its typical, large breathing modes as reported many times before.[2,3,9–11] One simulation of Notch100 (simulation 1) displayed slightly higher RMSD during the last 100 ns due to these movements of NCT-ECD. All subunits of the lipid bilayer remained stable after 200 ns. We also observe a notably broader distribution of fluctuations for PEN2 and Notch100 in the Notch complex vs. the C83 complex (**Figure**

S2-S3). PEN2, the smallest subunit of the complex, plays a role in the auto-proteolytic cleavage of HL2 between the TM6 and TM7, which produces the mature γ-Secretase complex.[9]

The overall dynamic changes in the shape and compactness of the systems during the full time course of the simulations were measured using R_g and SASA as summarized in **Figure S4**. The membrane-bound γ-secretase-substrate complexes were stable within the range of 39.3−40.3 Å; the experimental R_g values of 6IYC and 6IDF are computed to be 39.5 and 39.6 Å, respectively (labelled in magenta lines in **Figure S4**). The SASA for both the systems was also relatively constant within the range of 611−623 nm^2 after 200 ns, indicating minor changes in overall solvent exposure of the structural ensembles, which is largely controlled by the NCT ECD. The SASA values for the experimental 6IYC and 6IDF are computed to be 606 nm^2 (hydrophobic: 265 nm^2 and hydrophilic: 331 nm^2) and 620 nm^2 (hydrophobic: 276 nm^2 and hydrophilic: 331 nm^2) respectively (as shown in **Figure S4** with straight lines in magenta; note that the hydrophobic and hydrophilic do not sum perfectly to the total SASA as they were computed from two distinct GROMCAS tools). The substrate-bound systems remained more compact than the apo systems[3]. The statistics summarizing the dynamic stability of the complex systems are summarized in **Table S1**.

In order to compare the simulated and experimental structures directly, we performed a structural overlay of the cryo-EM structures and the most representative snapshot structures obtained from RMSD based cluster analysis (**Figure 2C-2D**). The Cα-RMSD of the γ-secretase-C83 complex with respect to experimental structure 6IYC is 1.80, 2.19 and 1.86 Å, respectively, whereas for the γ-secretase-Notch100 complex, it is 1.62, 1.68 and 1.64 Å for the three replicas respectively. In addition to these full-protein RMSD values of 1.62−2.19 Å, comparison of 6IYC with our simulated γ-secretase-C83 complex[1] gave Cα-RMSD values of 1.11, 1.17 and 1.45 Å for NCT, 1.23, 1.38 and 1.33 Å for PS1, 1.21, 1.32 and 1.02 Å for APH1-A, 0.80, 0.67 and 1.8 Å for PEN2, and 2.20, 3.10, and 2.41 Å for the substrate C83. For the γ-secretase-Notch100 complexes simulated in the present work, the Cα-RMSD values of the top three clusters relative to 6IDF are 1.18, 1.12, and 1.11 Å for NCT, 1.13, 1.40 and 1.54 Å for PS1, 1.18, 1.39, and 1.20 Å for APH1-A, 0.95, 0.85 and 1.18 Å for PEN2, and 2.40, 2.21, and 2.10 Å for Notch100, indicating similar accuracy for both protein systems. Considering the resolution of the experimental cryo-

EM data, this implies that the substrate structures are identical within the noise to the cryo-EM structures for the backbone atoms that can be directly compared. This ensures that our discussion of the 303-K dynamics of substrate-enzyme interactions occur in a context of close agreement with the experimental topology.

Figures

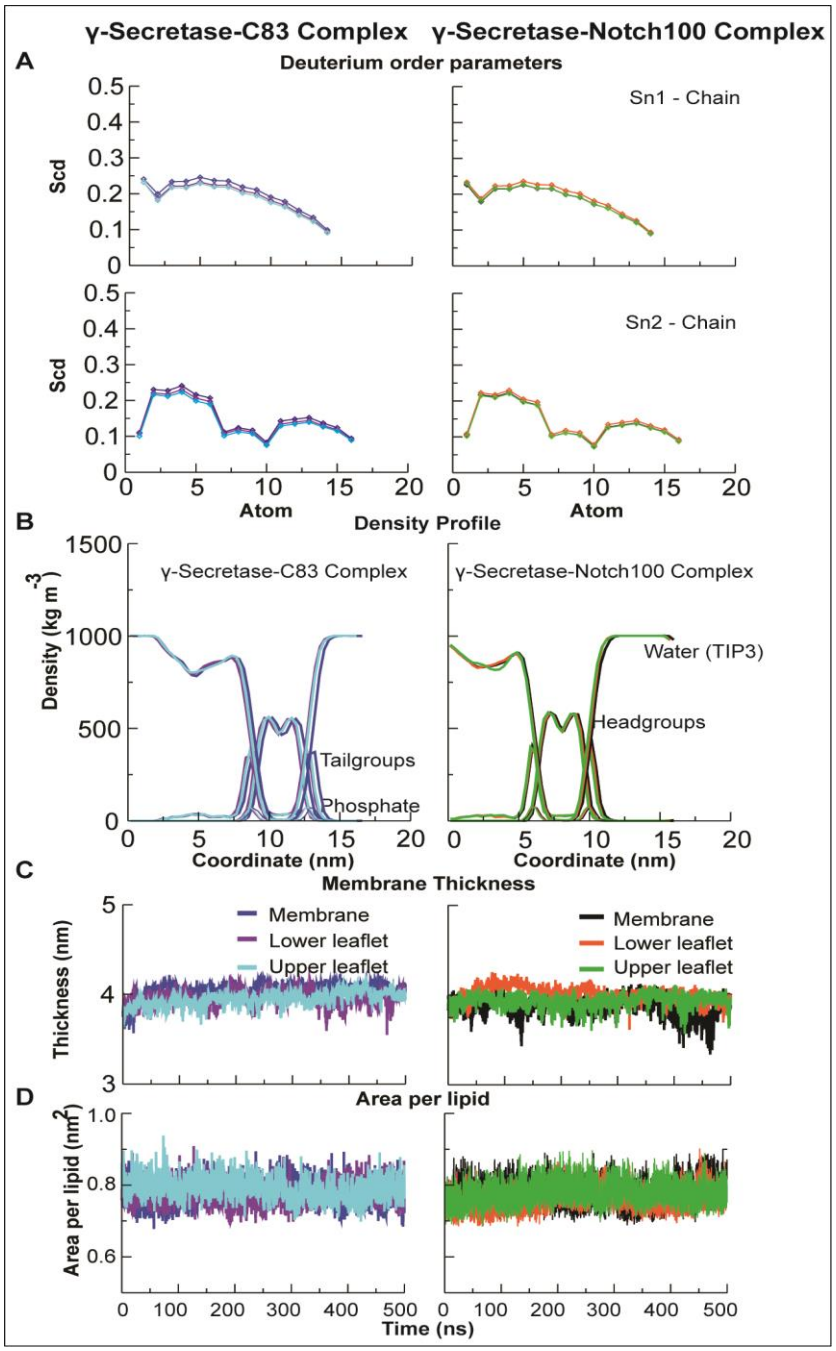

Figure S1. Membrane properties of γ-secretase-C83 and Notch100 bilayer systems averaged over each of the triplicate 500-ns MD simulations. Blue, purple, and cyan colors represent the three independent simulations for γ-secretase-C83. Black, orange, and green color represent the three independent simulations for γ-secretase-Notch100. (**A**) The order parameter distributions of Sn-1 and Sn-2 chains of the POPC lipids. (**B**) The density profiles of lipid headgroups, tail groups, phosphate and water (TIP3P) of the bilayer systems. (**C**) The average membrane thickness. (**D**) Area per lipid.

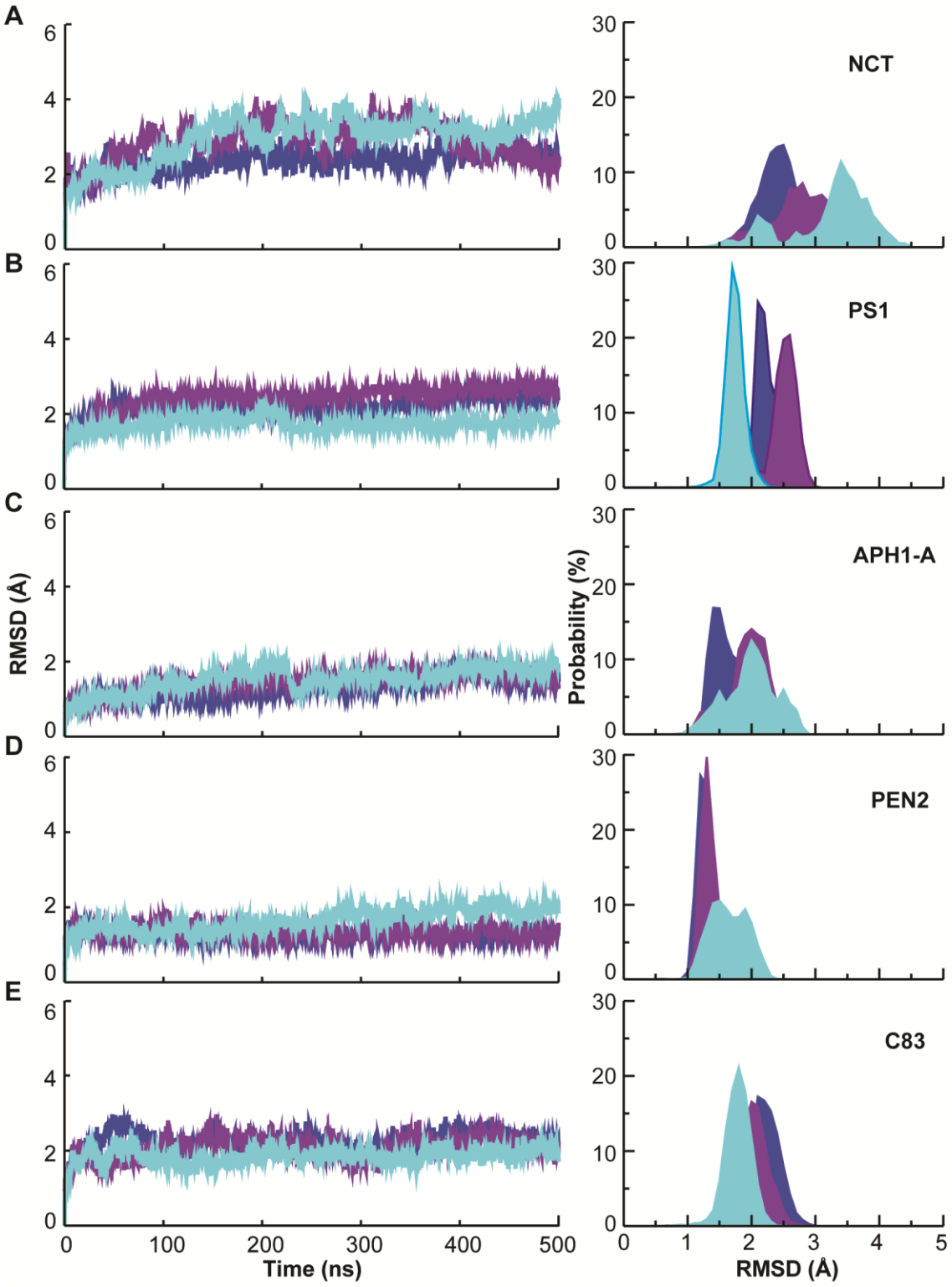

Figure S2. Room-temperature structural dynamics of C83-bound γ-secretase. Backbone root-mean-squared deviations from initial structures (RMSD) of the Notch100 substrate and four protein complex subunits i.e., Nicastrin, PS1, APH1-A, PEN2 and C83 for the three independent simulations (Blue: Simulation 1, Purple: Simulation 2 and Cyan: Simulation 3).

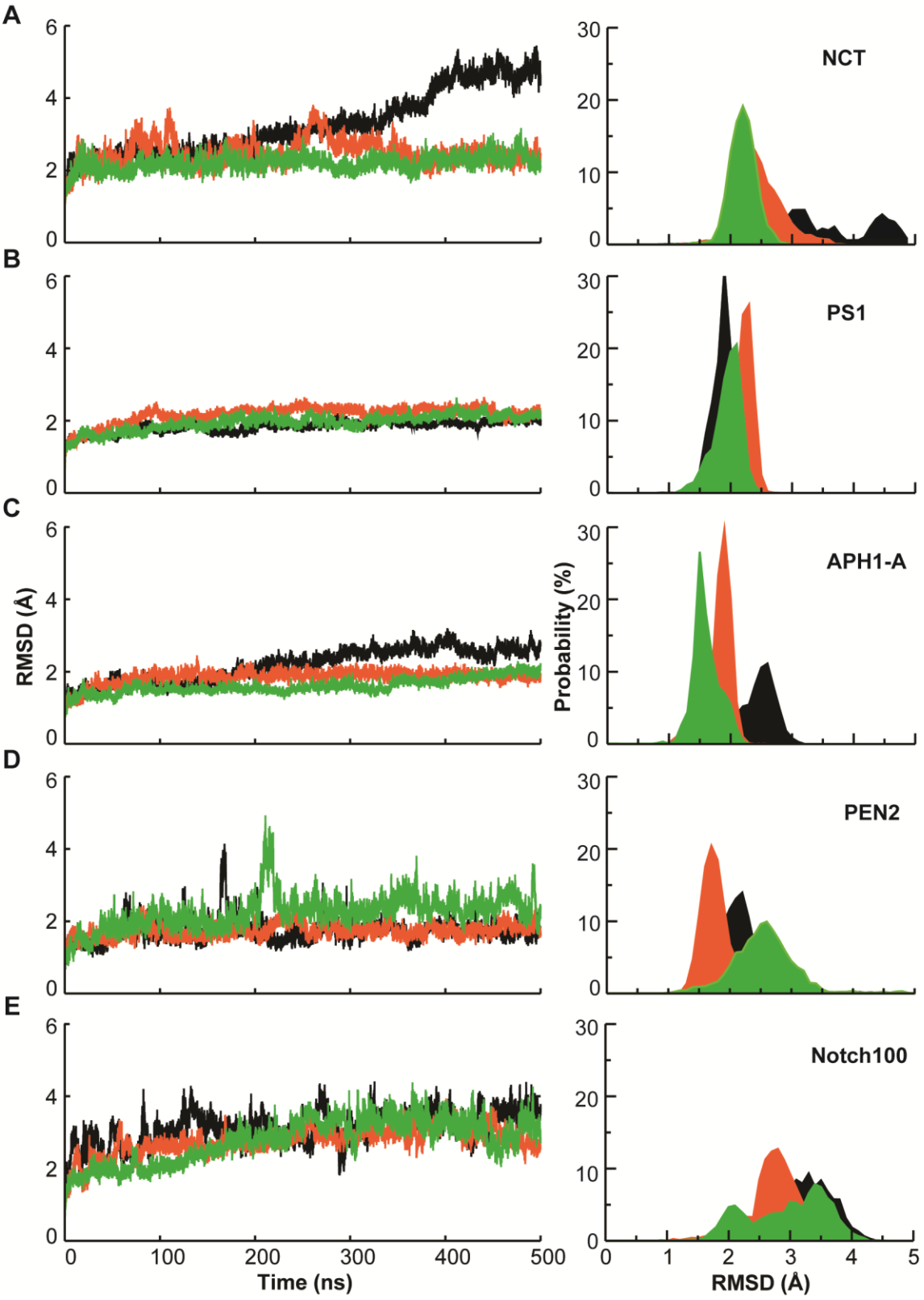

Figure S3. Room-temperature structural dynamics of Notch-bound γ-secretase. Backbone root-mean-squared deviations from initial structures (RMSD) of the Notch100 substrate and four protein complex subunits i.e., Nicastrin, PS1, APH1-A, PEN2 and Notch100 for the three independent simulations (Black: Simulation 1, Orange: Simulation 2 and Green: Simulation 3).

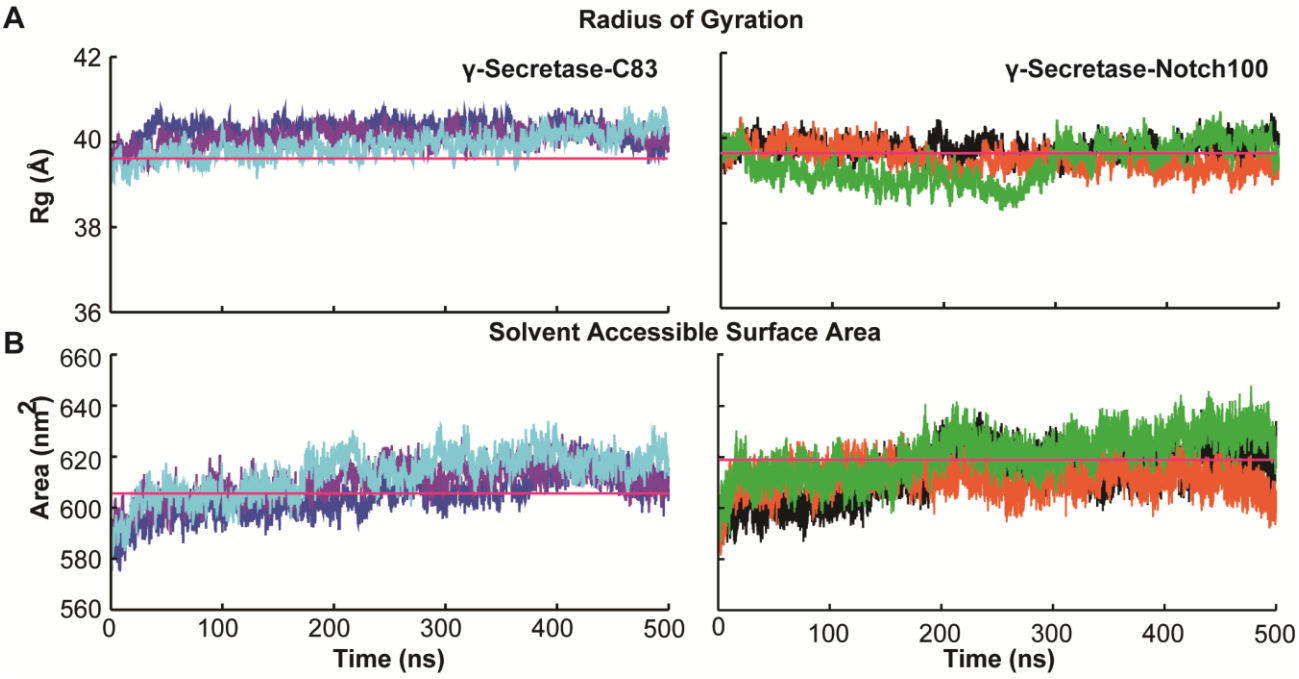

Figure S4. Evolution of the radius of gyration (R_g) and solvent accessible surface area (SASA) of the γ-secretase-C83 and Notch100 complexes during the full simulations. (**A**) Radius of gyration. (**B**) solvent-accessible surface area. The blue, purple and cyan colors represent the three independent simulations for the γ-seecretase-C83 complex. The black, orange and green color represents the three independent simulations for the γ-secretase-Notch100 complex. The straight magenta line in each figure depicts the R_g and SASA of experimental cryo-EM structures γ-seecretase-C83 (6IYC) and γ-secretase-Notch100 (6IDF) complex.

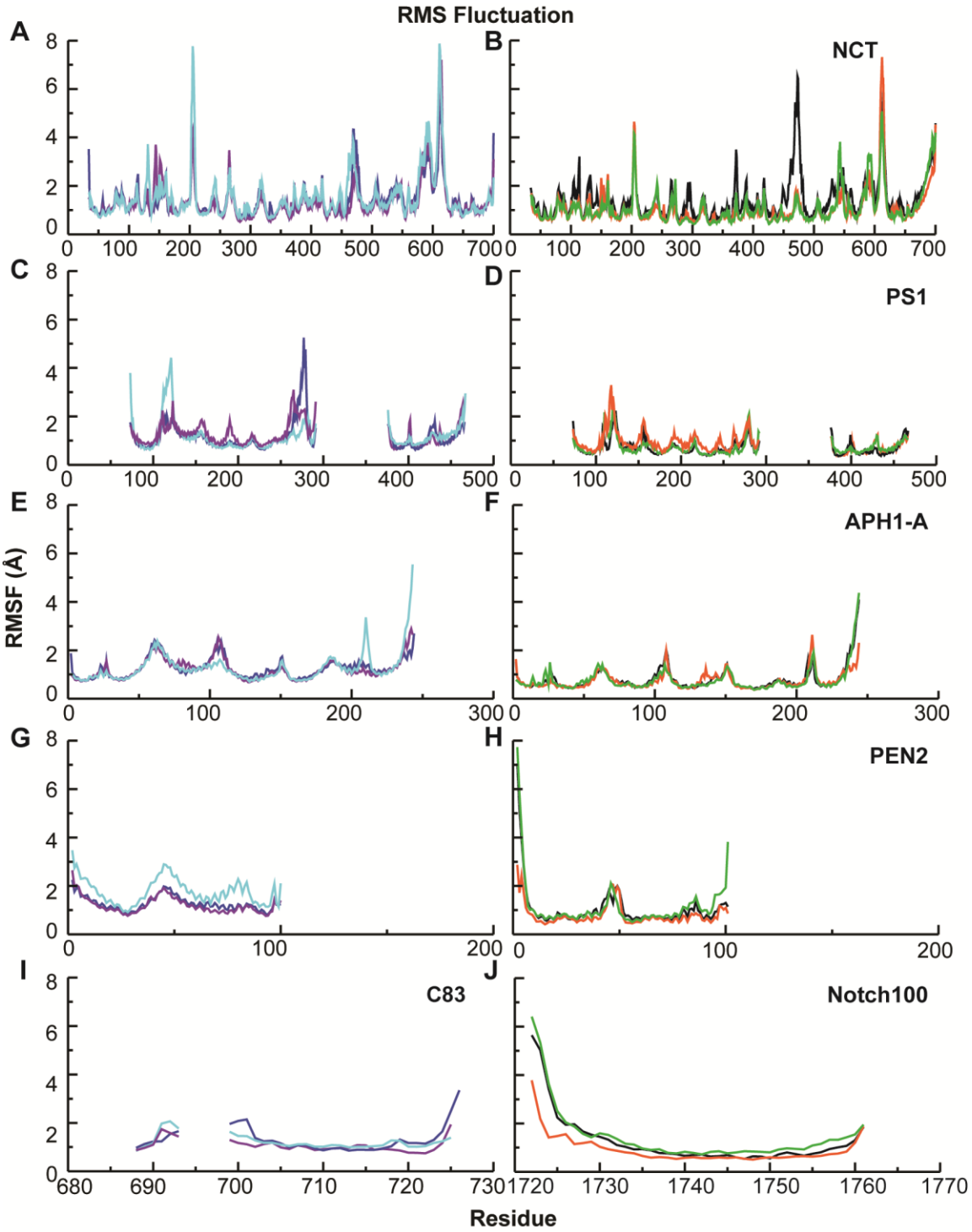

Figure S5. The Cα RMSF analysis of subunits of γ-secretase-C83 and Notch100 complexes. The blue, purple, and cyan lines represent the RMSF for simulation 1, 2, and 3 of γ-secretase-C83. The black, orange, and green lines represent the RMSD for simulation 1, 2, and 3 of γ-secretase-Notch100. **Left Panel**: (**A**) Cα-RMSF of Nicastrin (**C**) Cα-RMSF of PS1, (**E**) Cα-RMSF of APH1-A (**G**) Cα-RMSF of PEN2 (**I**) Cα-RMSF of C83. **Right Panel**: (**B**) Cα-RMSF of Nicastrin (**D**) Cα-RMSF of PS1, (**F**) Cα-RMSF of APH1-A (**H**) Cα-RMSF of PEN2 (**J**) Cα-RMSF of Notch100.

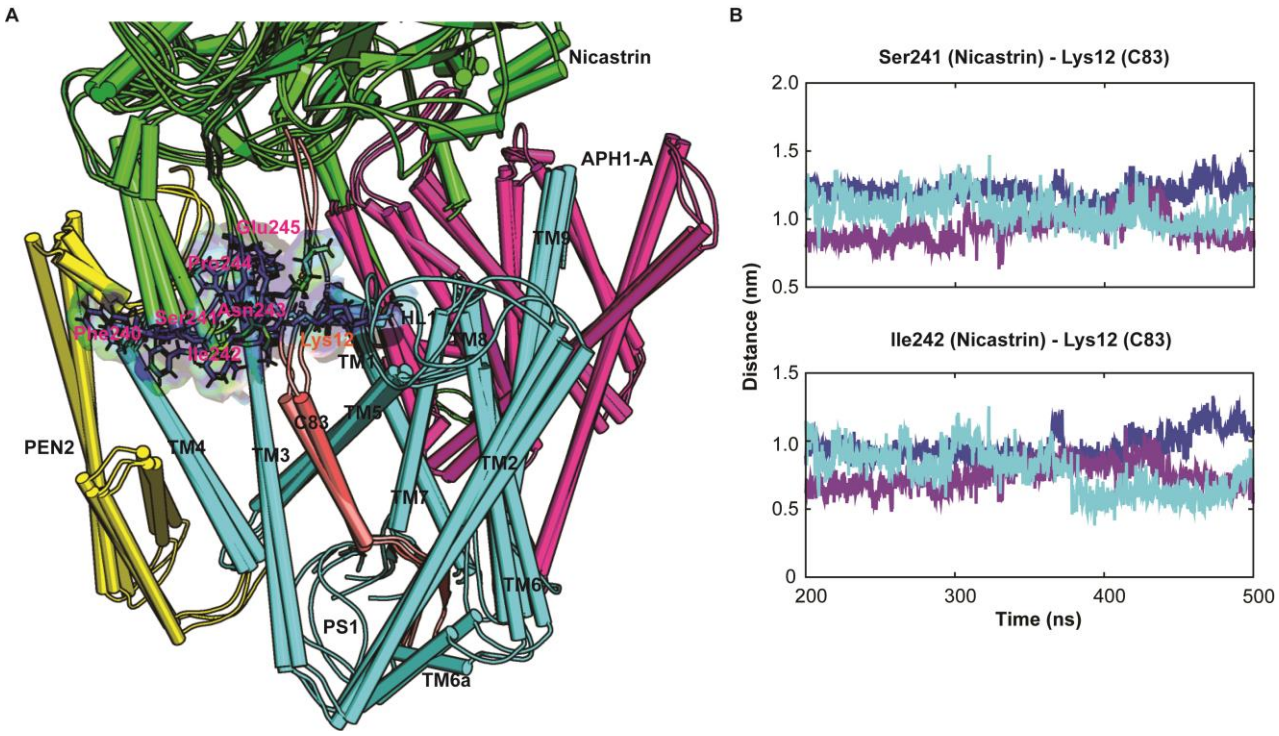

Figure S6. Structural overlay of γ-secreatse-C83 complexes obtained from cluster analysis along with position of the NCT ECD interface (Phe240-Glu245) and Lys12 (corresponds to Lys699 in APP) and minimum distance profile. The close proximity to the interface has TM1 and HL1 of PS1 which represents the binding site of some specific γ-secretase modulators which plays a major role in stability of the enzyme-substrate complex as well as subsequent cleavage.

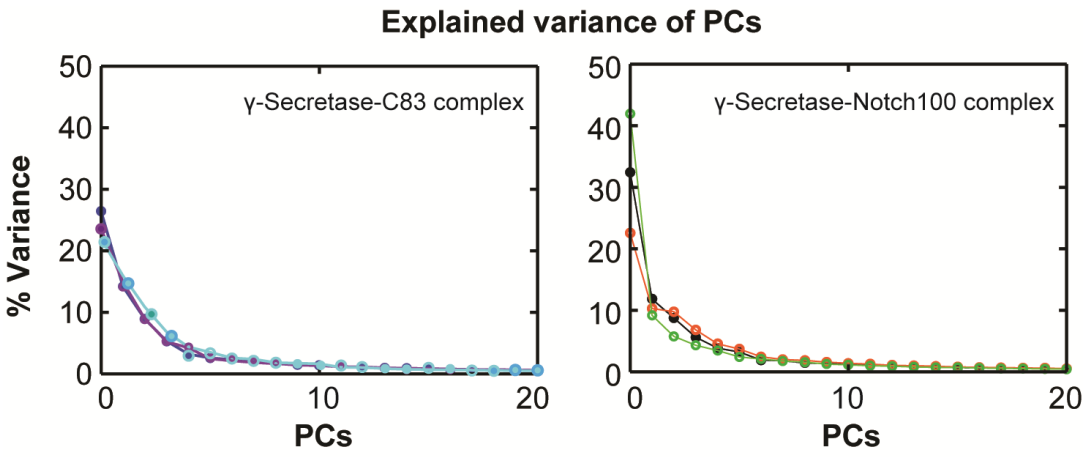

Figure S7. Principal component analysis of the γ-secretase-C83 and Notch100 complexes using CA atoms using the last 300 ns of the trajectories. Left Panel: The explained variation for the first 20 PCs of γ-secretase-C83 complexes (The blue, purple and cyan lines represent simulations 1, 2, and 3, respectively). **Right Panel**: The explained variation for the first 20 PCs of γ-secretase-Notch100 complexes (The black, orange and green lines represent simulations 1, 2, and 3, respectively).

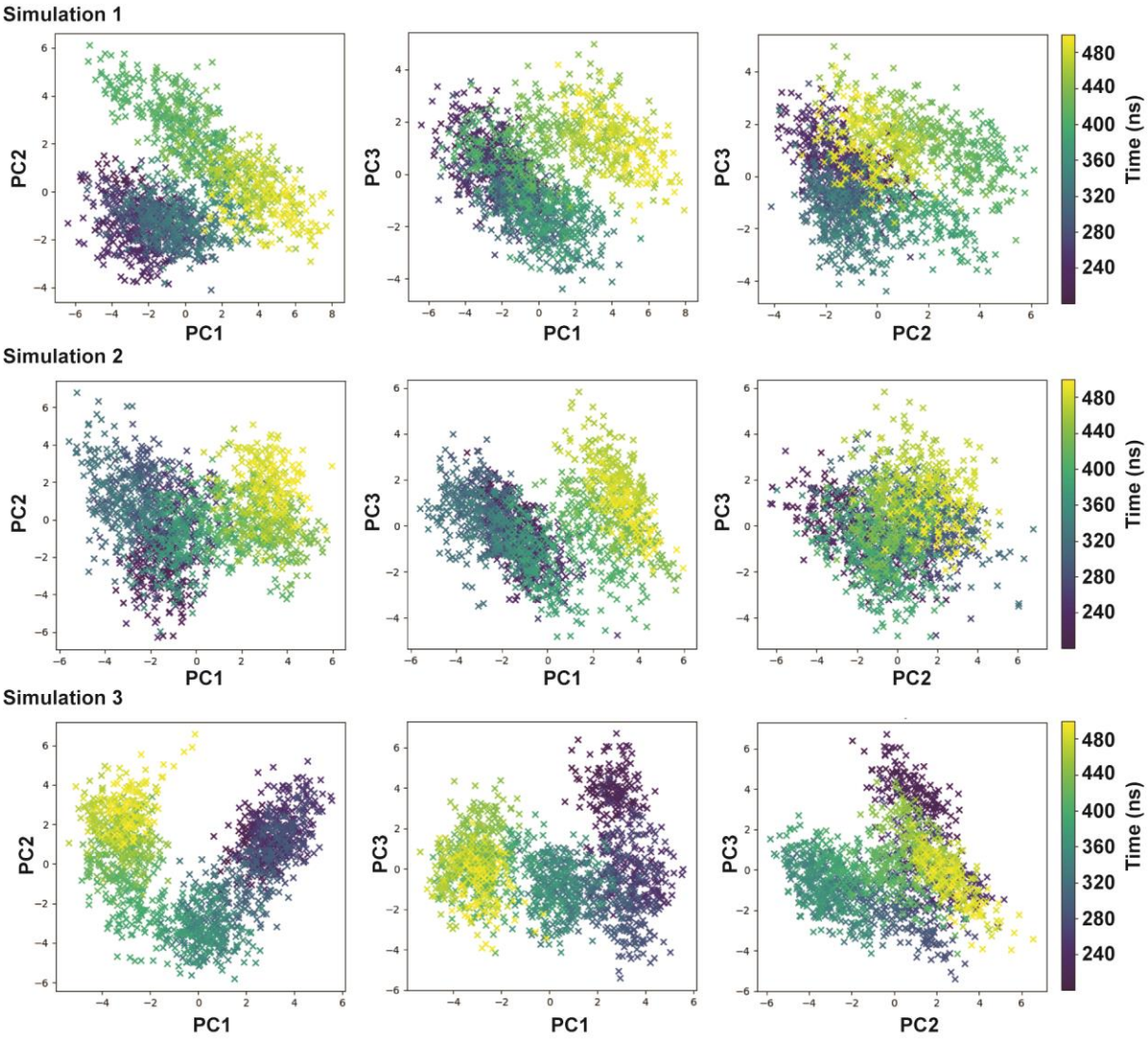

Figure S8. The 2D projection plots of first three principal components of γ-secretase-C83.

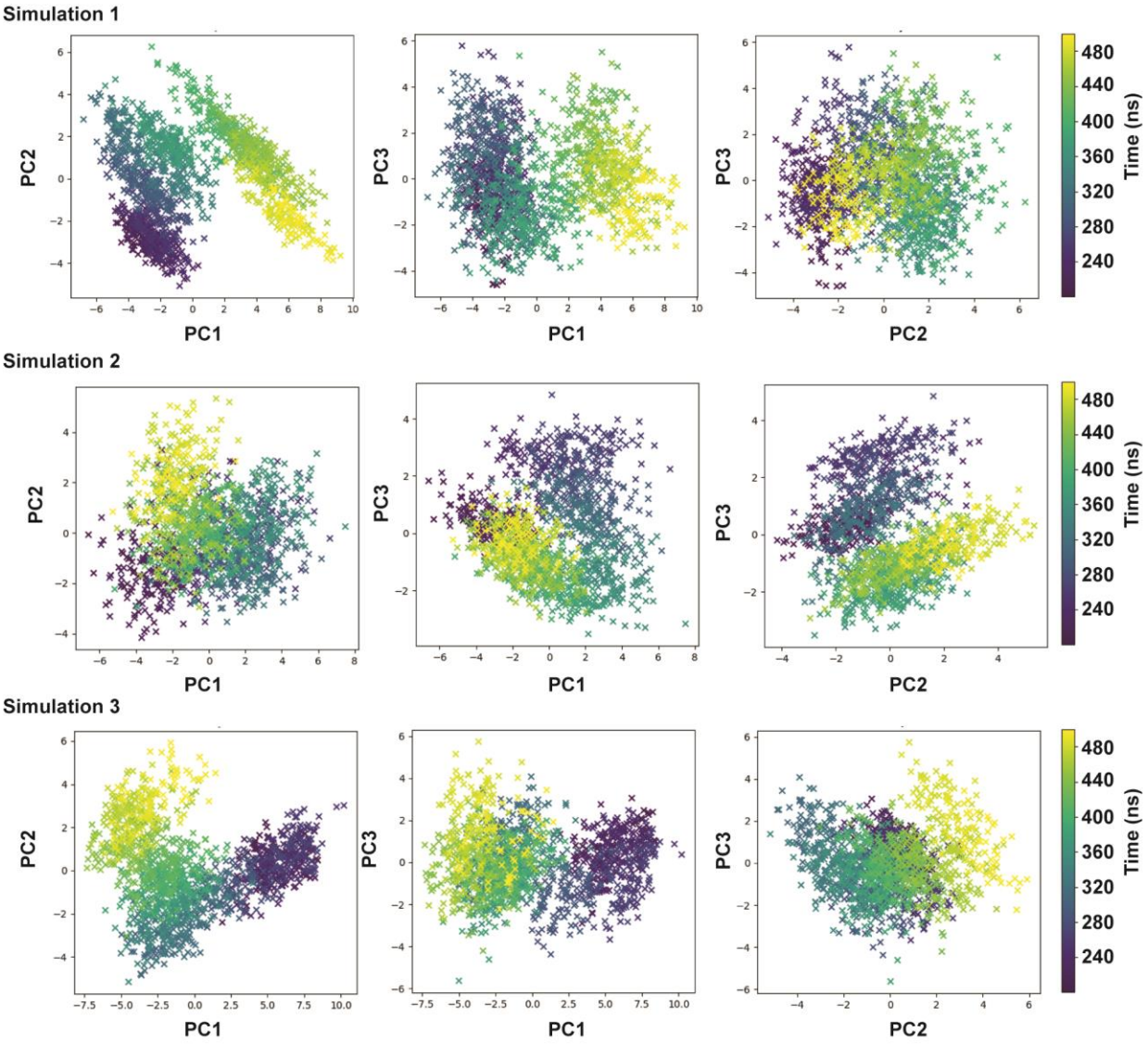

Figure S9. The 2D projection plots of first three principal components of γ-secretase-Notch100.

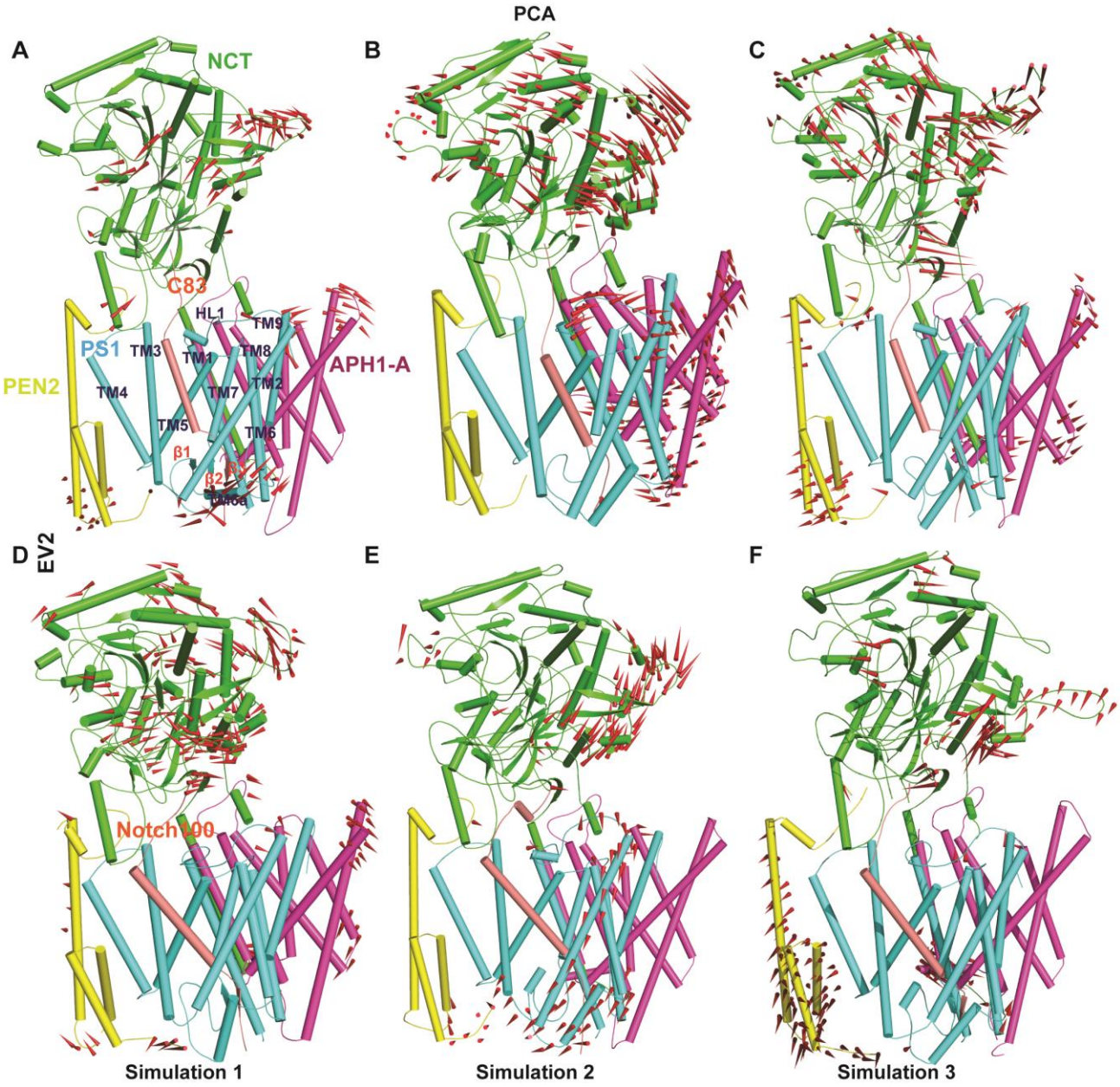

Figure S10. Atomic motions of the enzyme-substrate complexes. Porcupine plots displaying the main motions of the subunits of γ-secretase-C83 and Notch100 complexes extracted from the top-two eigenvectors (EV2) of the last 300 ns of each trajectory. **A-C**) the movement of the Nicastrin (green), Presenilin1 (Cyan), APH1-A (Purple), PEN2 (Yellow) and C83 (tint grey) of γ-secretase-C83 for simulation 1 (A), 2, (B), and 3 (C). **D-F**) the movement of the Nicastrin, PS1, APH1-A, PEN2 and Notch100 (tint grey) of γ-secretase-Notch100 for simulation 1 (D), 2, (E), and 3 (F). The red arrows represent the direction of motion and the lengths depict the amplitude of motion. Most notably, apart from Nicastrin ECD, PEN2 and APH1-A subunits displayed high movement in γ-secretase-C83 (Figure S7-B) and γ-secretase-Notch100 (Figure S7-F).

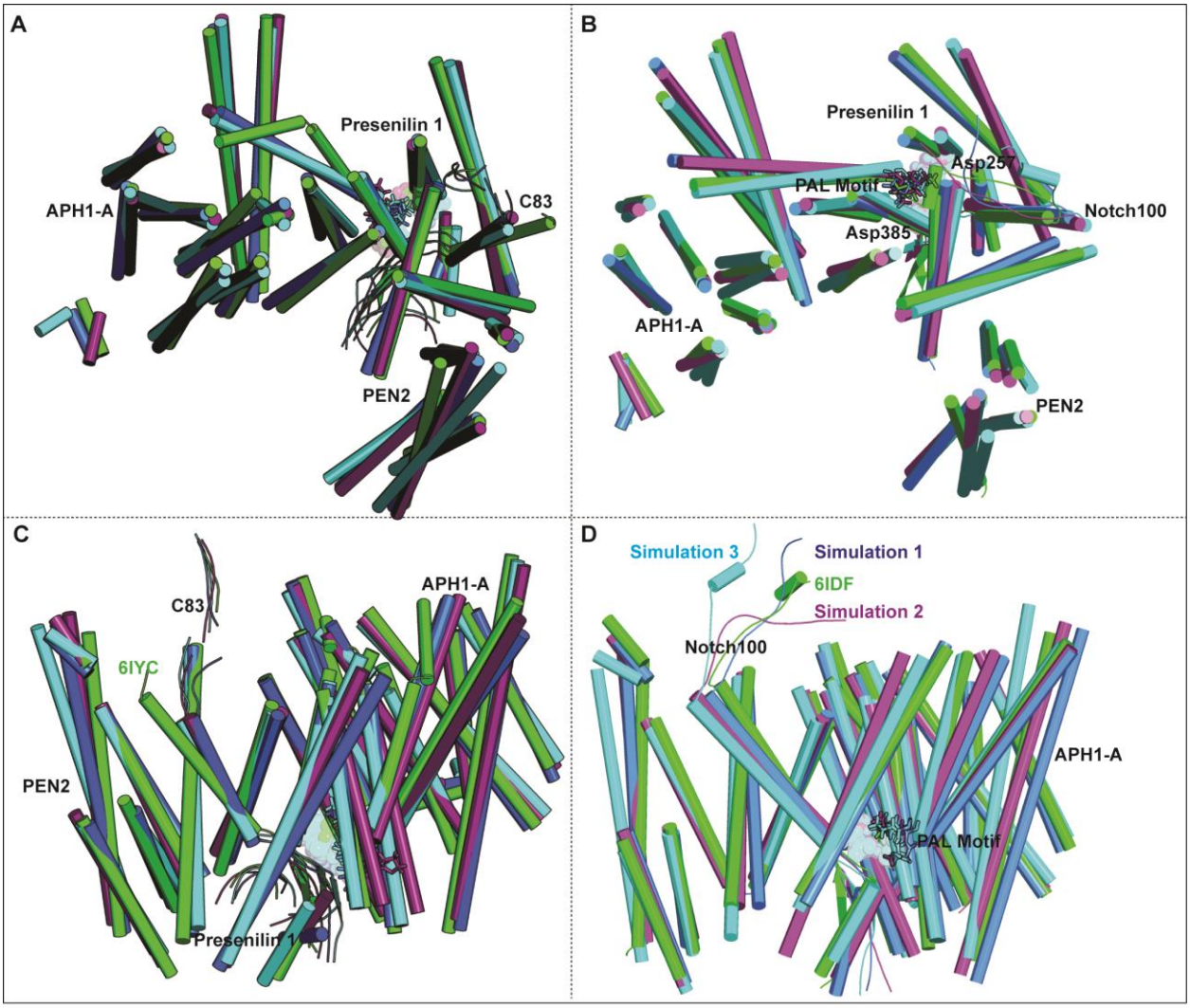

Figure S11. Comparative analysis of TM helices. The helix properties of nicastrin, presenilin 1, APH1-A, PEN2 and the substrates C83 and Notch100 were obtained from cluster analysis and compared to experimental cryo-EM structures**.** (**A**) Superimposed top view of γ-secretase-C83 and Notch100 complexes. (**B**) Superimposed bottom view of experimental γ-secretase-C83 and Notch100 complexes. Green color represents experimental cryo-EM structures of the γ-secretase-C83 and Notch100 complexes (6iYC and 6IDF). (**C**) As (A), but sideward perspective. (**D**) As B, but sideward perspective. Blue, purple, and light blue depict representative cluster structures from simulation 1, 2 and 3, respectively.

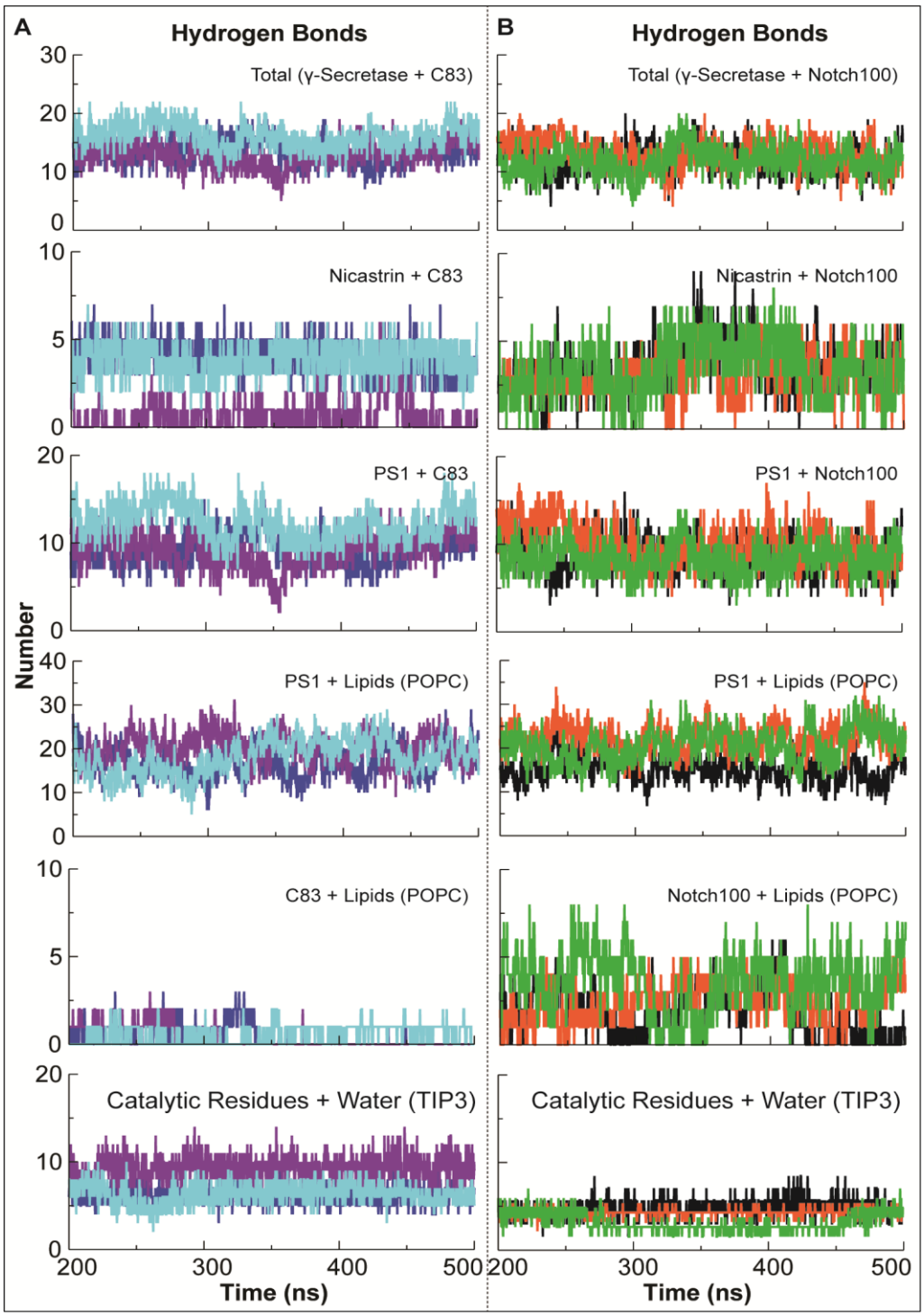

Figure S12. Inter-molecular hydrogen bond dynamics of γ-secretase-C83 and -Notch100 complexes. (**A**) Dynamic stability of the γ-secretase-C83 complex portraying the distinct hydrogen bonding between different sub-units, including C83 and lipids. (**B**) Corresponding dynamic stability of hydrogen bonds of the γ-secretase-Notch100 complex.

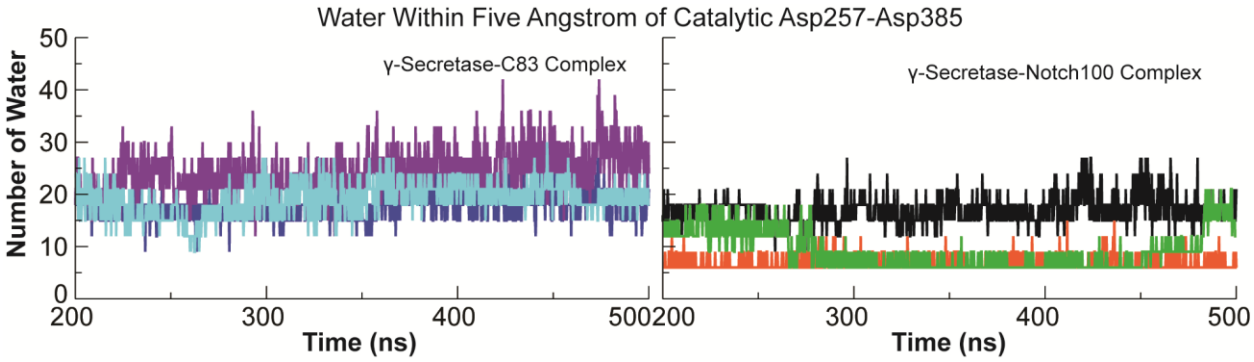

Figure S13. Dynamics of water accessibility by the catalytic aspartates (Asp257 and Asp385) of γ-secretase-C83 and Notch100 complexes (last 300 ns). The graph depicts the number of water molecules that are accessible to the catalytic site (within 5 Å).

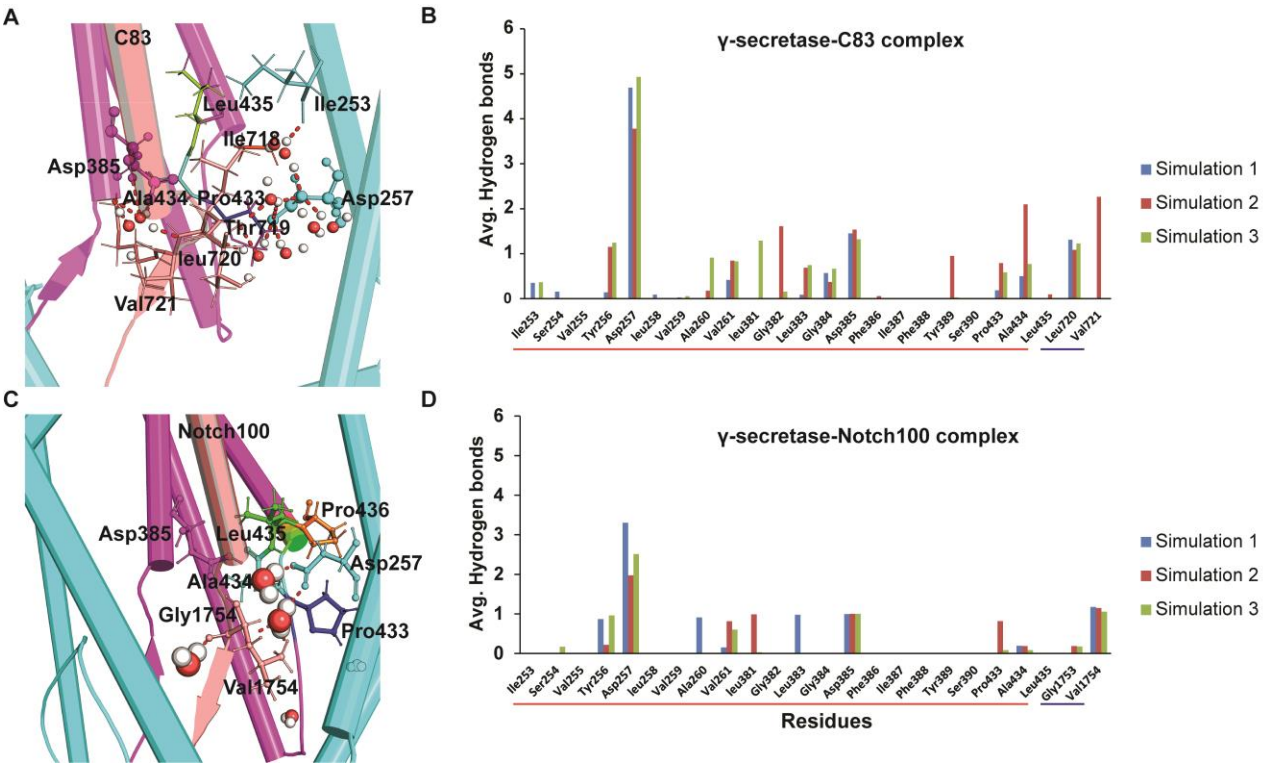

Figure S14. **Differential accessibility of water mediated hydrogen bonds by the residues surrounding the catalytic site of PS1 in γ-secretase-C83 and -Notch100 complexes.** (**A**) Water hydrogen bonds to catalytic and surrounding residues within 5 Å in the γ-secretase-C83 complex (Asp257: Cyan and Asp385: magenta while PAL motif blue, cyan and green). (**B**) Average number of hydrogen bonds formed between water and the catalytic pocket residues (per frame in trajectory) in γ-secretase-C83. (**C**) Snapshot showing the water mediated hydrogen bonds with the catalytic residue and surrounding residues within 5 Å in γ-secretase-Notch100 (**D**) Average number of hydrogen bonds formed between water and the catalytic pocket residues in γ-secretase-Notch100.

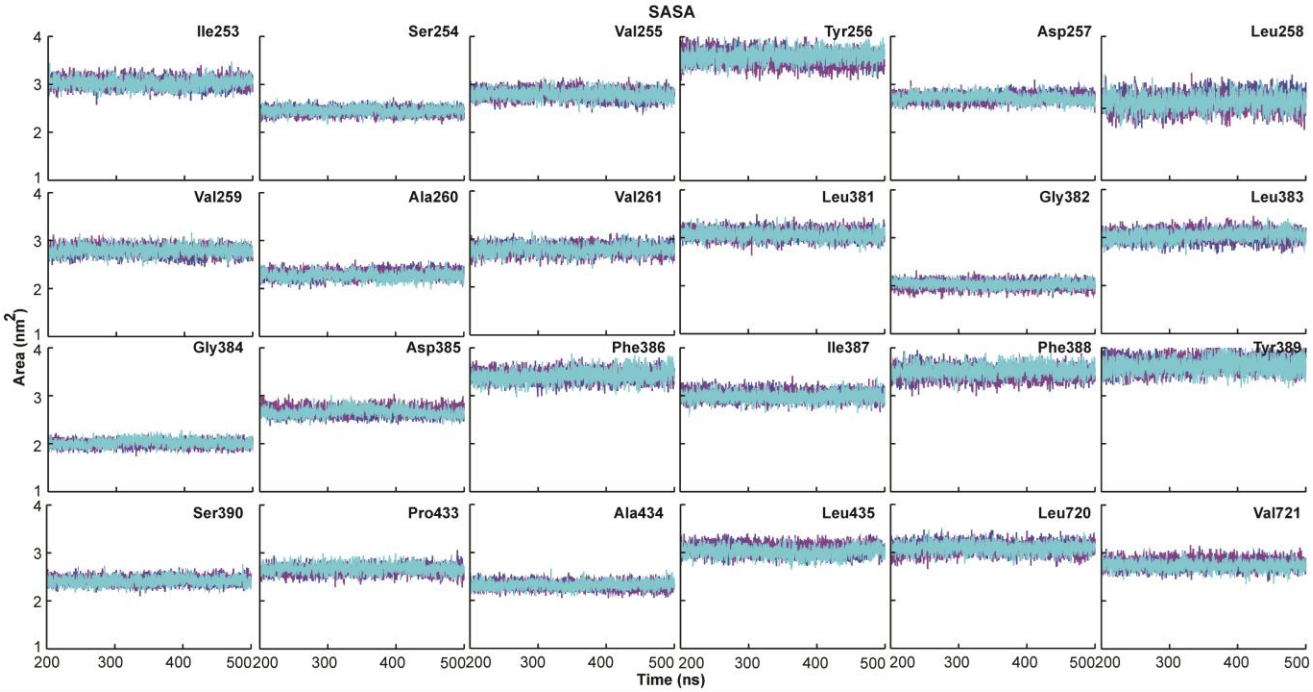

Figure S15. Solvent accessible surface area of the residues surrounding the catalytic Aspartates (residues within 5 Å of Asp253 and Asp385 of PS1) displaying the differential solvent exposure in γ-secretase-C83 bound complex systems during the last 300 ns MD.

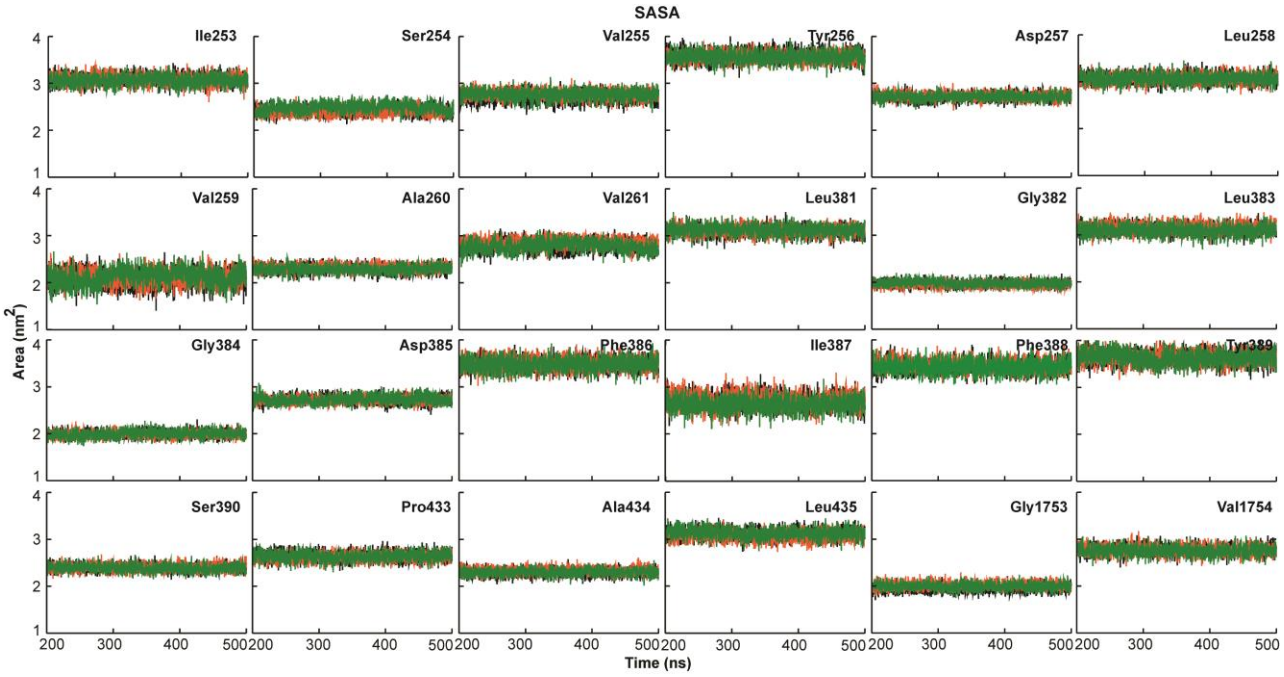

Figure S16. Solvent accessible surface area of the residues surrounding the catalytic Aspartates (residues within 5 Å of Asp253 and Asp385 of PS1) displaying the differential solvent exposure in γ-secretase-Notch100 bound complex systems during the last 300 ns MD.

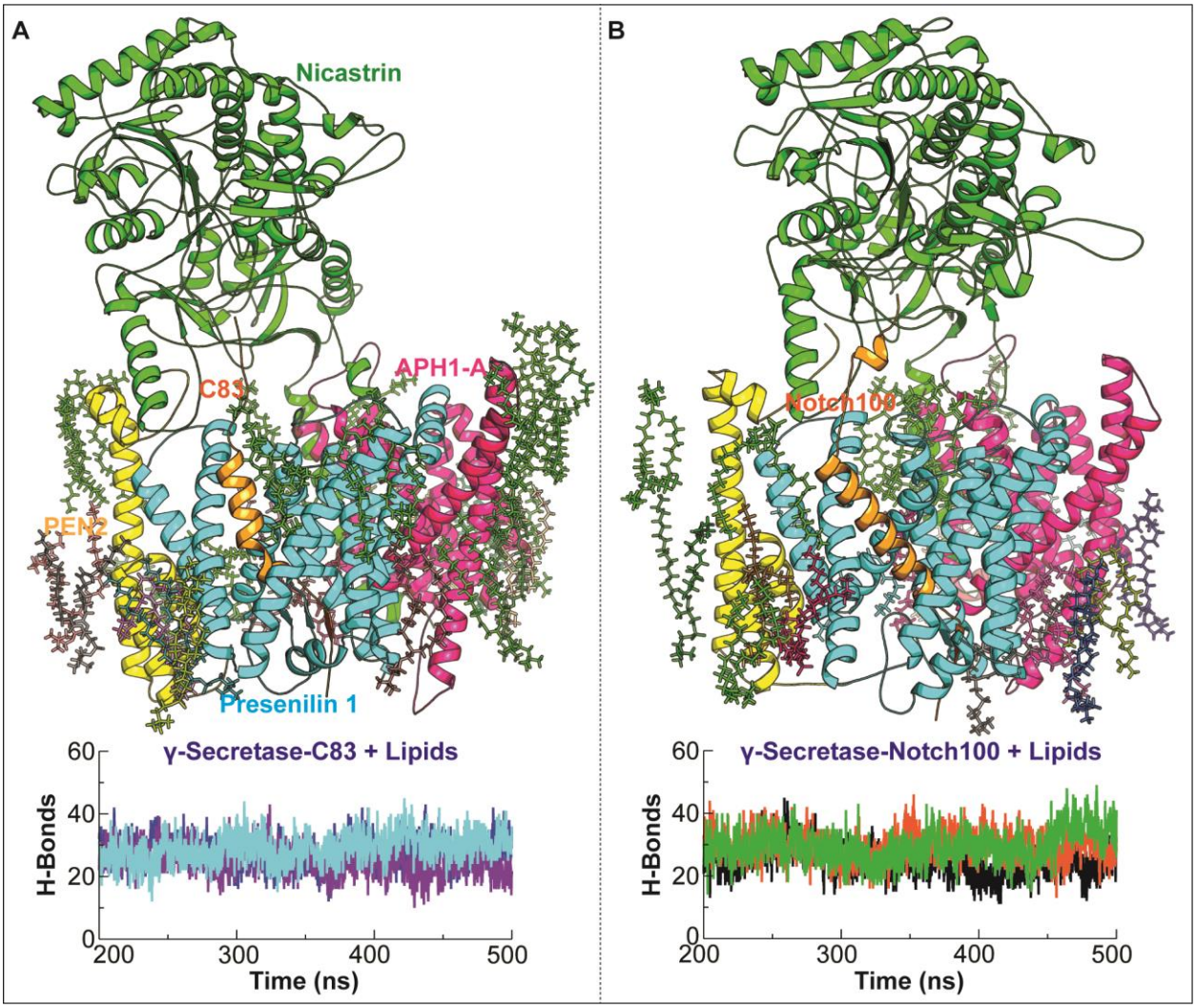

Figure S17. Differential preference of binding of POPC lipids in γ-secretase-C83 and Notch100 complexes. (**A**) Lipid binding sites in γ-secretase-C83. (**B**) Lipid binding sites in γ-secretase-Notch100. The analysis is based on the occupancy (>=20%) of lipids binding to the different sites computed using the last 300 ns trajectory of each simulation system. The lower panels show the lipid-protein hydrogen-bond dynamics of two complex systems during the last 300 ns.

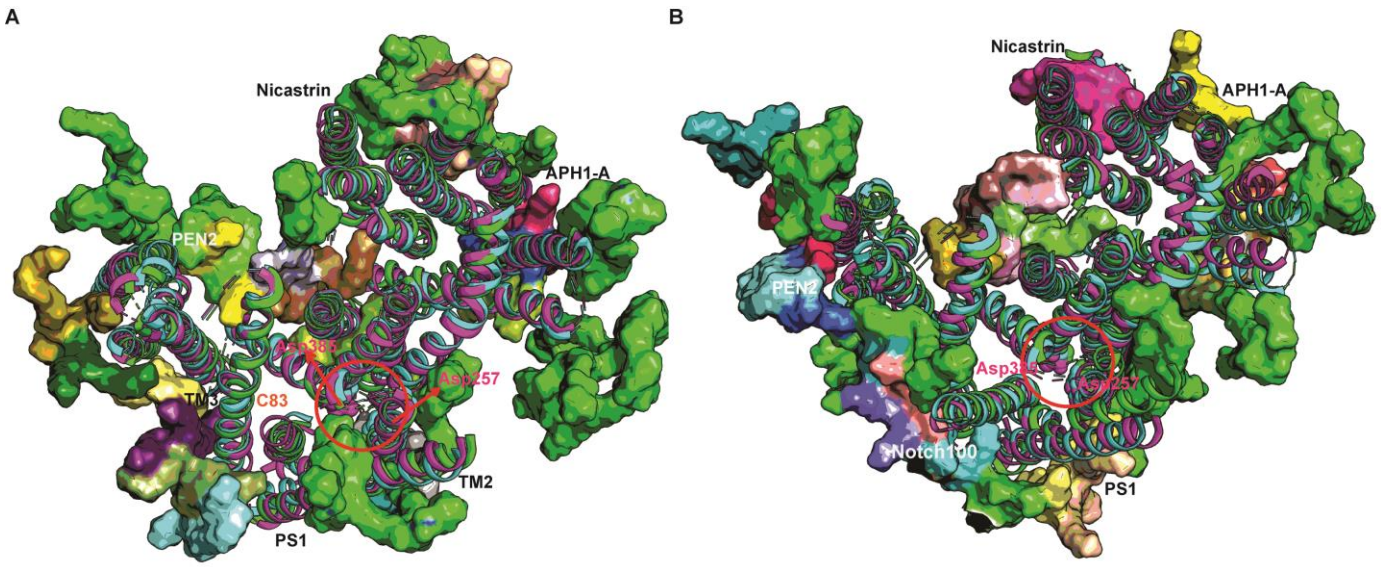

Figure S18. **Lipid binding sites. A)** γ-secretase-C83. **B)** γ-secretase-Notch100. For clarity, we have only displayed the TM regions of each sub-units of γ-secretase.

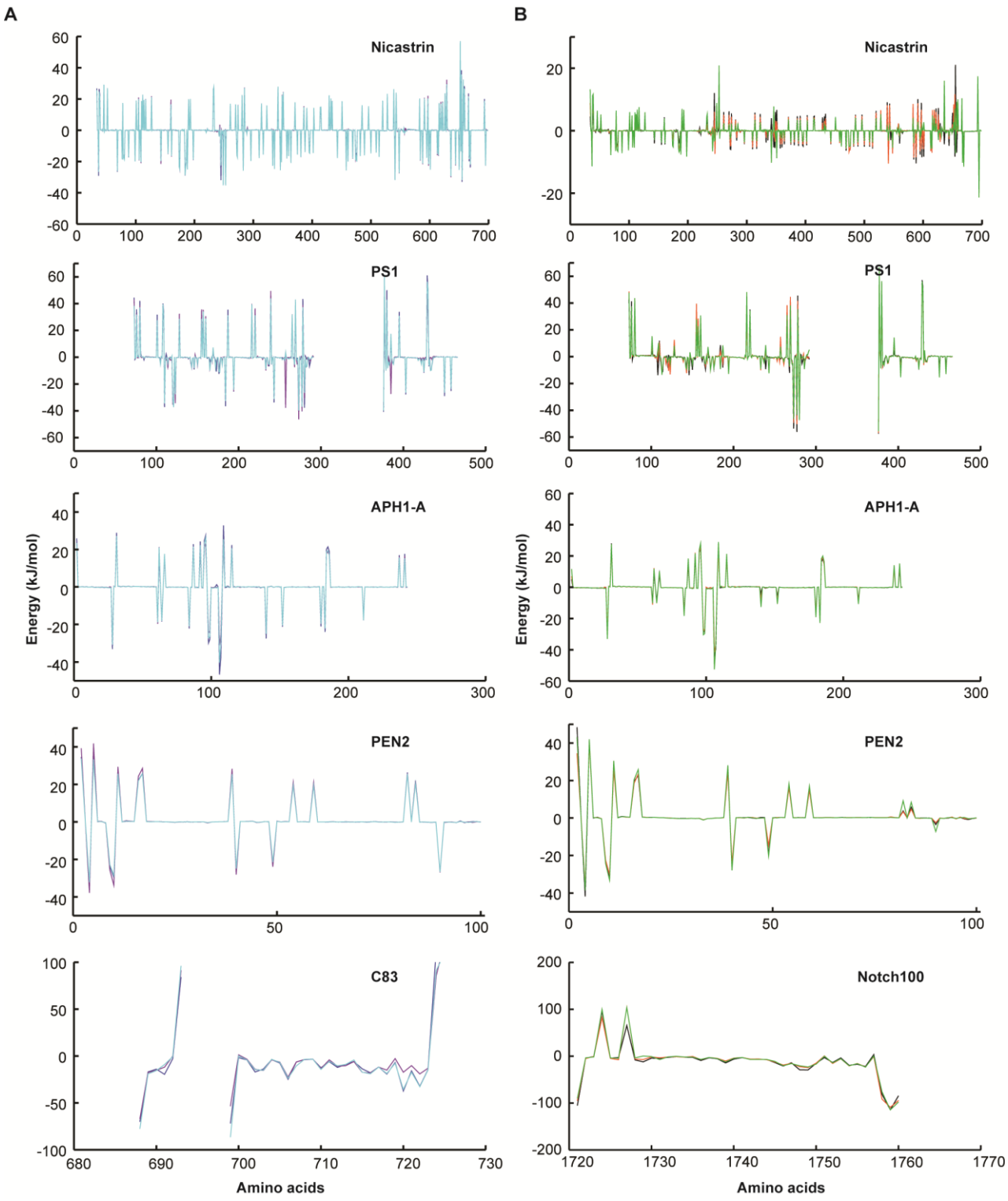

Figure S19. **Per-residue free energy decomposition for γ-secretase-C83 and -Notch100 based on MM/PBSA calculations (last 300 ns). (A)** γ-secretase-C83 complex showing three independent simulations (blue: simulation 1, purple: simulation 2 and cyan: simulation 3). **(B)** γ-secretase-Notch100 complex showing three independent simulations (black: simulation 1, orange: simulation 2 and green: simulation 3).

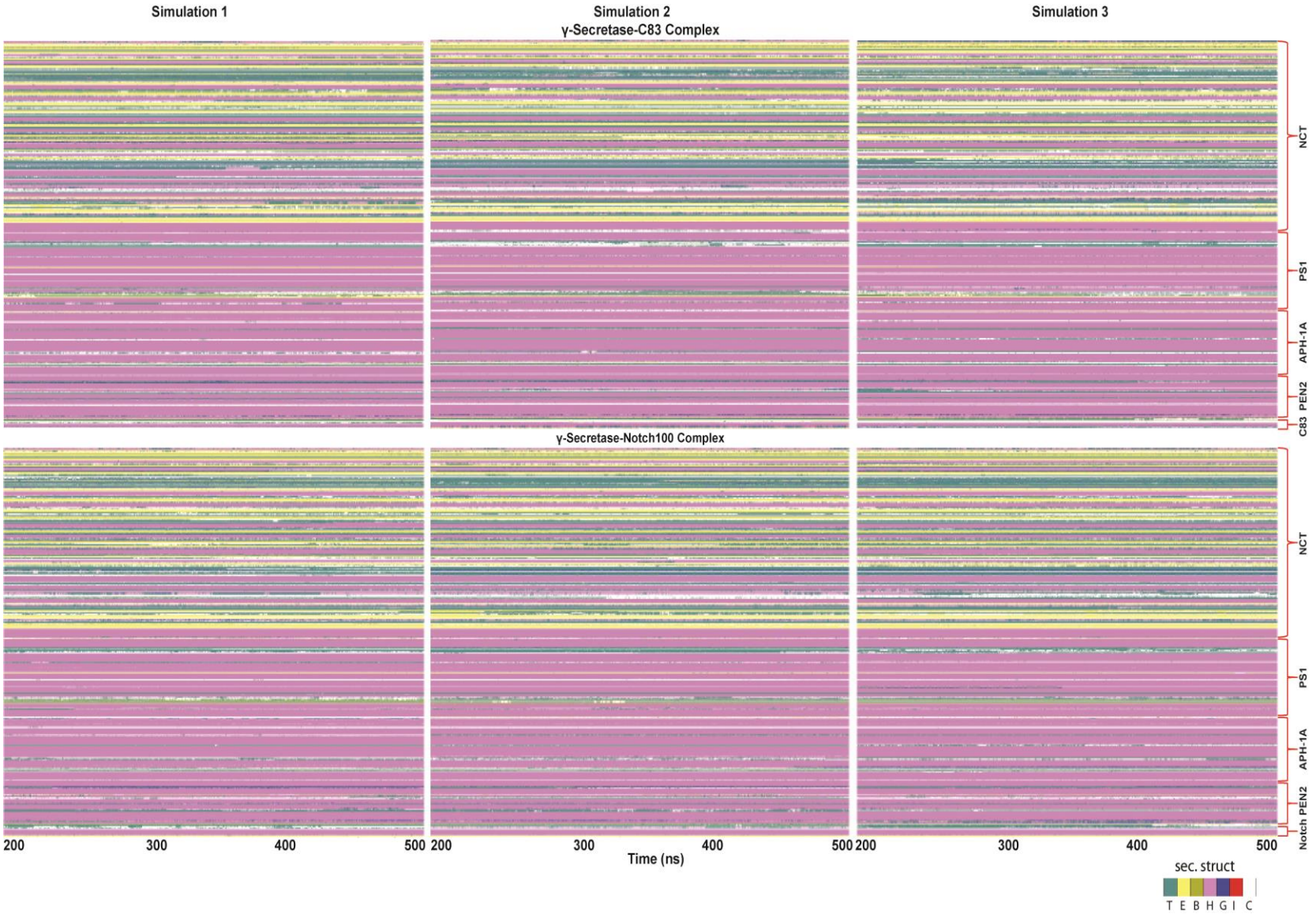

Figure S20. Evolution of secondary structure elements in C83 and Notch100 bound γ-secretase conformations during the last 300 ns MD. Upper Panel: Evolution of the different sub-units of C83 bound γ-secretase complex**. Lower Panel:** Evolution of the different sub-units of **Notch100** bound γ-secretase complex.

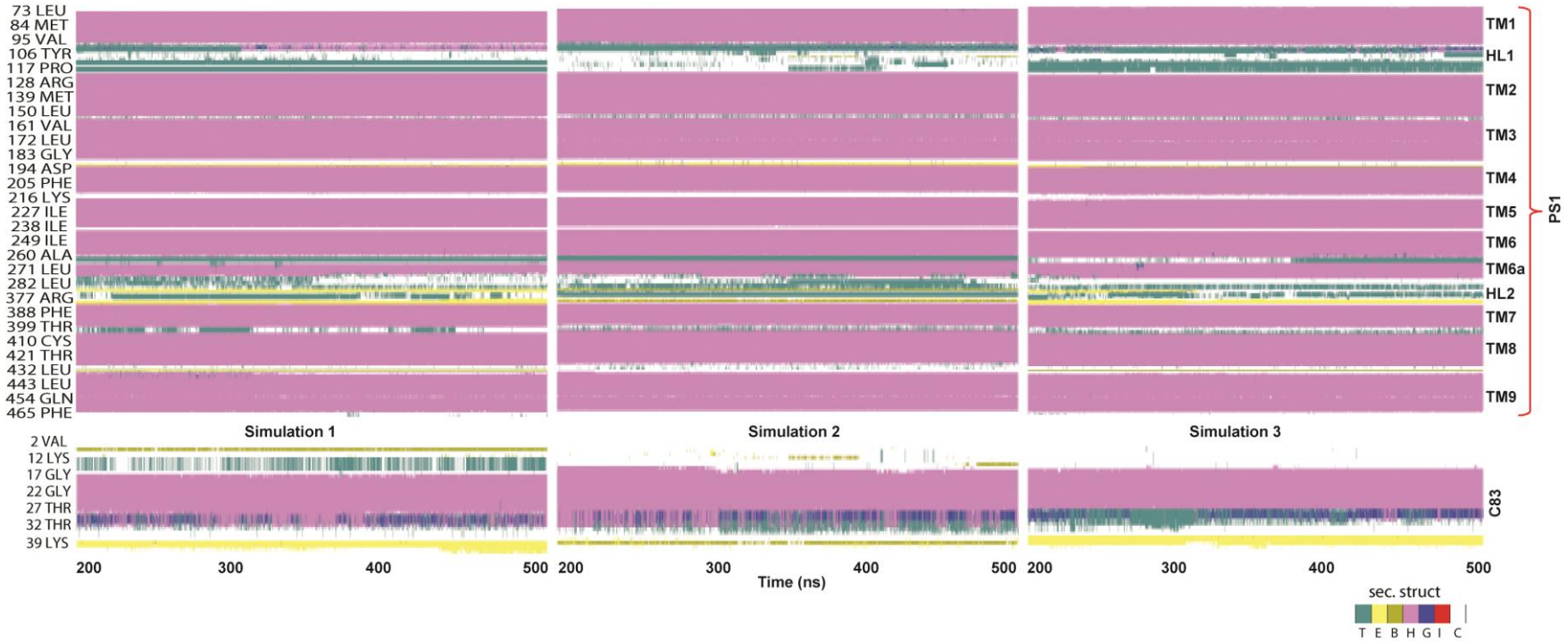

Figure S21. Zoomed in view displaying the evolution of secondary structure elements of catalytic PS1 and substrate C83 in γ-secretase-C83 bound complexes during MD.

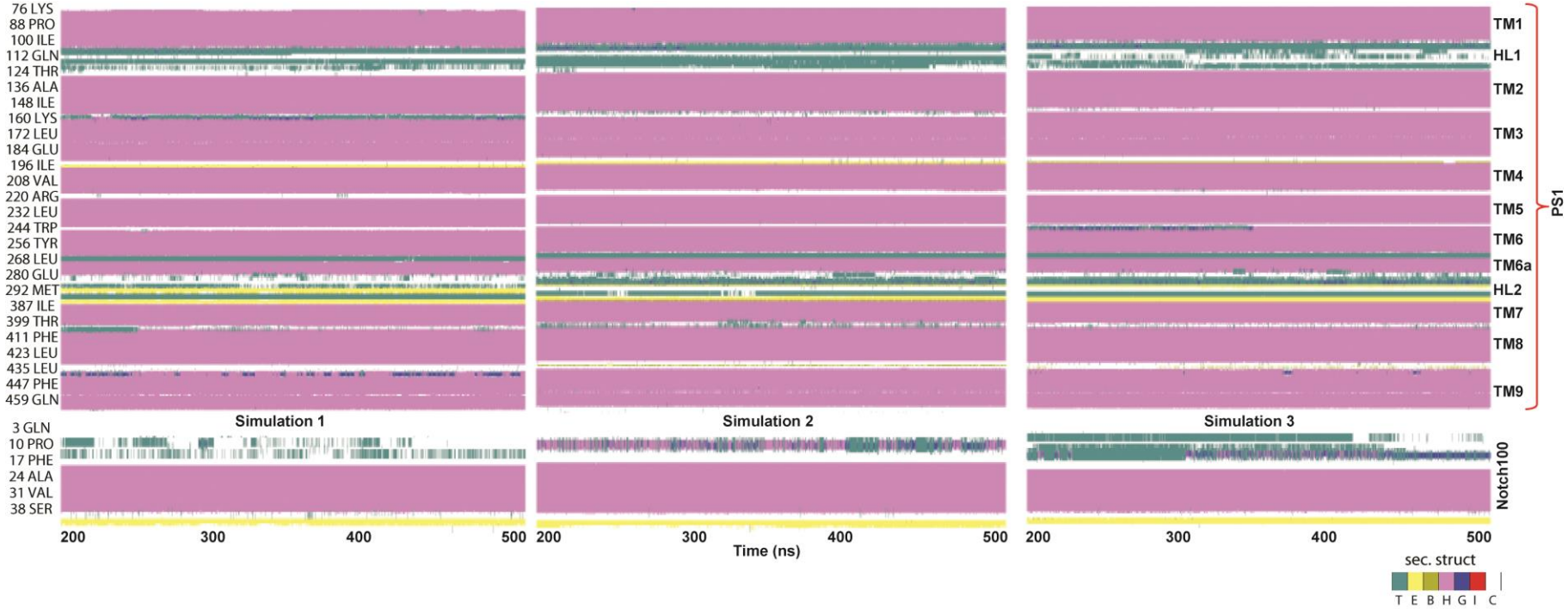

Figure S22. Zoomed in view displaying the evolution of secondary structure elements of catalytic PS1 and substrate Notch100 in γ-secretase-Notch100 bound complexes during MD. The image was rendered using VMD timeline.

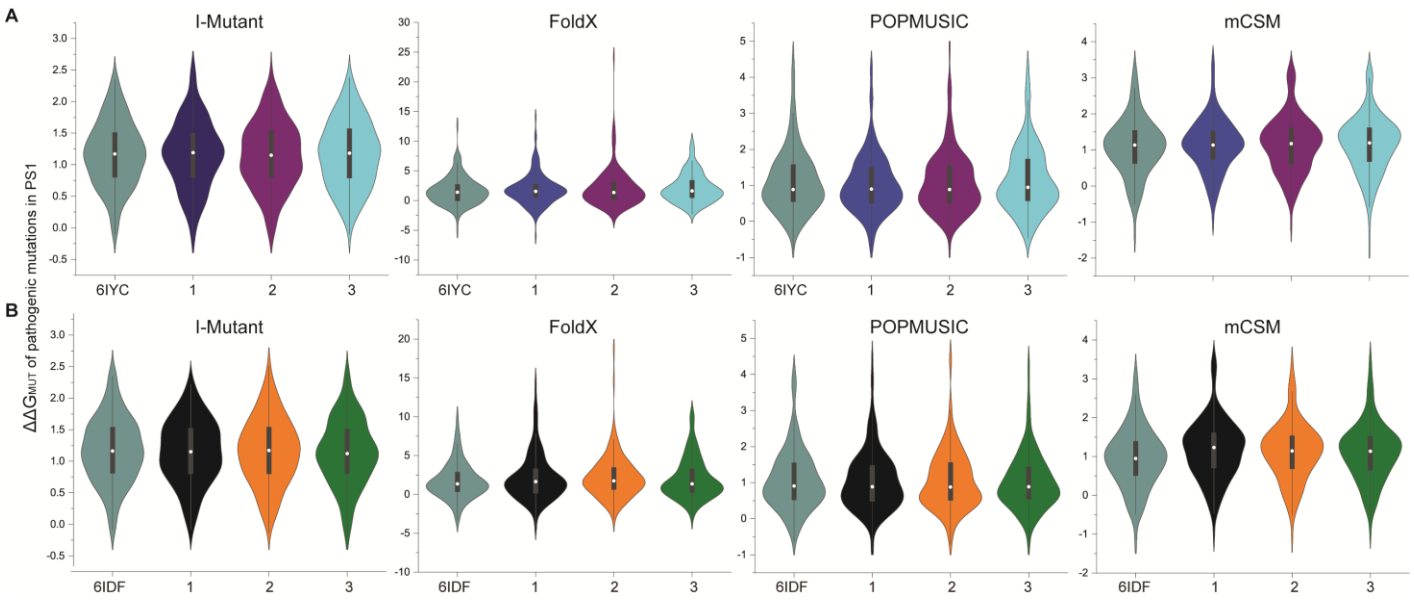

Figure S23. The distribution of computed $\Delta\Delta G_{MUT}$ values for 149 pathogenic PS1 mutations in substrate-bound γ-secretase using experimental and MD-simulated structures. (**A**) For C83-bound state (6IYC). (**B**) For Notch100-bound state (6IDF). 1: simulation 1, 2: simulation 2, and 3: simulation 3.

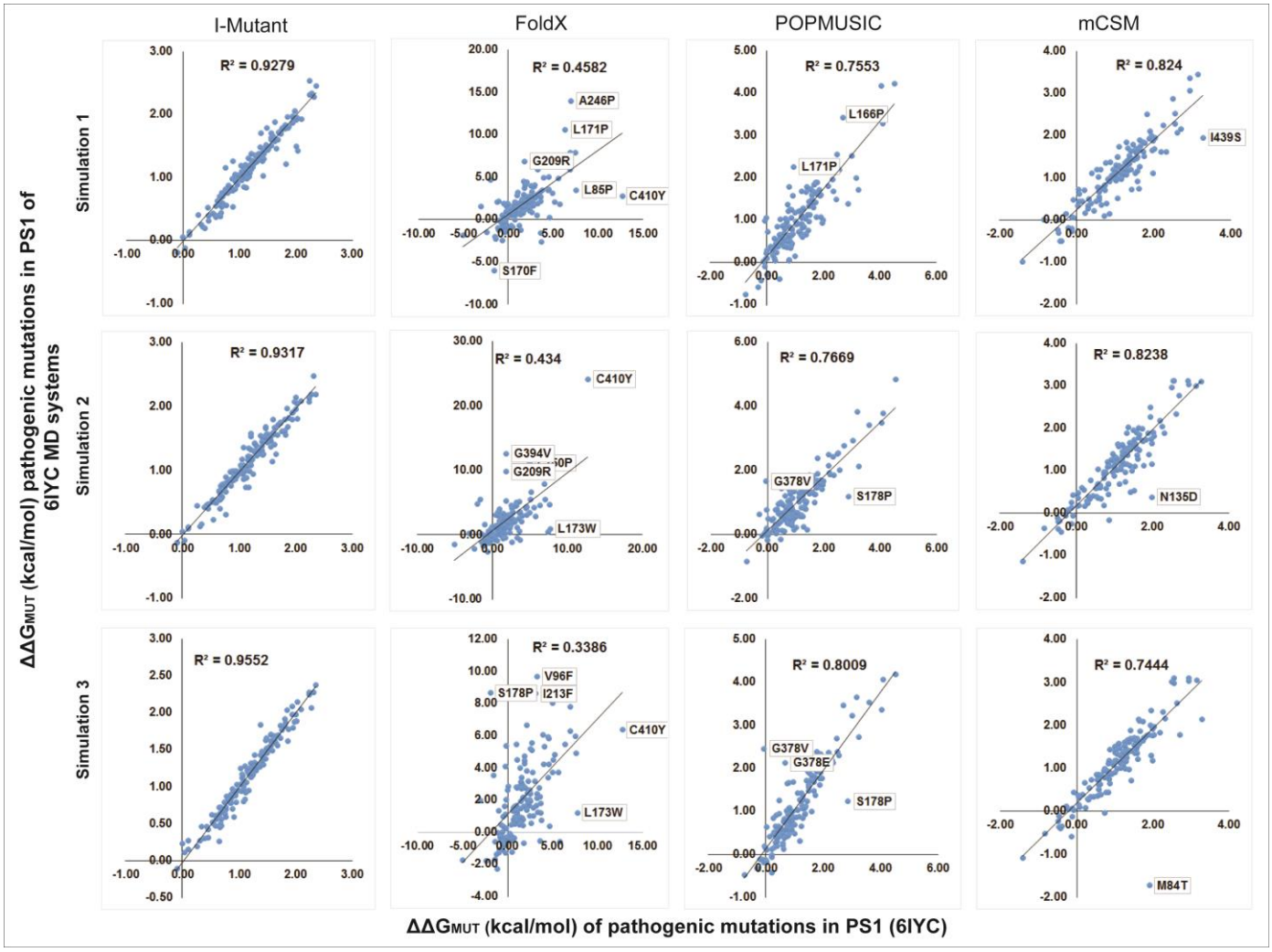

Figure S24. **Experimental vs. computed structure-based stability effects for C83-bound γ-secretase.** The figures show the relation between computed $\Delta\Delta G_{MUT}$ of pathogenic PS1 mutations on the C83 complex using the experimental structure 6IYC or the representative simulated structures obtained from cluster analysis from three independent MD simulations.

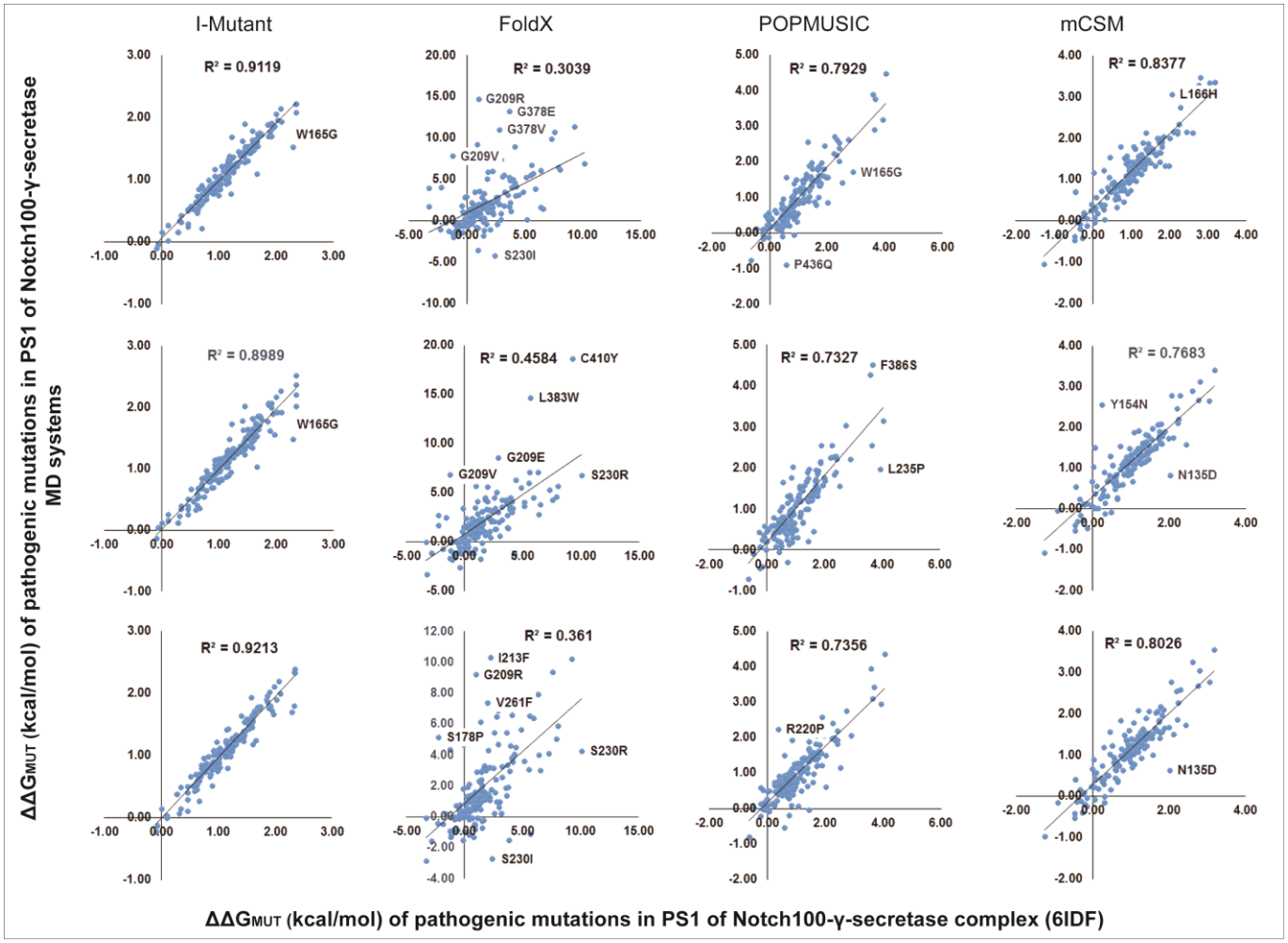

Figure S25. **Experimental vs. computed structure-based stability effects for Notch100-bound γ-secretase.** The figures show the relation between computed $\Delta\Delta G_{MUT}$ of pathogenic PS1 mutations on the Notch complex using the experimental structure 6IDF as compared to using representative simulated structures obtained from cluster analysis from three independent MD simulations.

Tables

Table S1. Comparative analysis of the Cα-RMSF of the key residues (in Å unit) in γ-Secretase C83 and Notch100 complex MD systems.

Systems	**Simulation**	**Catalytic Residues**		**PAL motif**		
		Asp257	**Asp385**	**Pro333**	**Ala434**	**Leu435**
C83	Simulation 1	0.99	0.66	0.84	1.26	1.13
	Simulation 2	0.93	0.81	0.88	1.22	1.11
	Simulation 3	1.24	0.88	0.84	1.00	1.04
Notch100	Simulation 1	0.52	0.37	0.66	0.58	0.47
	Simulation 2	0.39	0.36	0.40	0.34	0.37
	Simulation 3	0.53	0.54	0.64	0.66	0.59

Table S2. Lipid binding sites in the individual subunits of γ-secretase-substrate bound systems.

Lipid Binding Sites	C83 complex	Notch100 Complex
Nicastrin	Glu667, Leu670, Ile671, Thr674, Val675, Phe677, Gly678, Ile679, Phe682, Ile685, Val686, Cys689, Ile690, Leu697, Ile699	Leu670, Ile671, Val675, Phe677, Gly678, Ile679, Ile685, Val686, Cys689, Ile690, Lys693, Leu697, Ile699
PS1	Val87, Thr90, Leu91, Val95, Ala98, Lys101, Ser102, Gln112, Ile114, Tyr115, Val125, Arg128, Ala129, Leu130, Ile133, Leu134, Ile140, Ile143, Met146, Leu149, Trp165, Ile168, Ser169, Leu172, Leu173, Phe176, Phe177, Tyr181, Leu182, Tyr189, Leu201, Phe205, Arg220, Leu221, Arg224, Ile227, Met228, Met233, Val236, Tyr240, Glu243, Trp244, Leu248, Ile249, Val252, Thr256, Arg278, Asn279, Glu280, Trp404, Thr407, Ile408, Phe411, Gln454	Val87, Thr90, Leu91, Val95, Ala98, Lys101, Ser102, Gln112, Tyr115, Val125, Arg128, Ala129, Ile133, Leu134, Ile140, Val142, Ile143, Met146, Leu149, Trp165, Ile168, Ser169, Leu172, Leu173, Phe176, Phe177, Tyr181, Leu182, Tyr189, Leu201, Phe205, Arg220, Leu221, Arg224, Met233, Val236, Phe237, Tyr240, Glu243, Leu248, Ile249, Val252, Thr256, Arg278, Asn279, Thr407, Ile408, Phe411
APH1-A	Pro16, Leu20, Tyr119, Leu158, Thr159, Phe162, Leu169, Phe173, Tyr218, Val222, Leu226, Phe229, Leu236, Arg237, Ile239, Gln240, Ser242, Leu243, Leu244	Pro16, Leu20, Tyr119, Leu158, Thr159, Phe162, Leu169, Phe173, Leu215, Tyr218, Leu226, Phe229, Ile239, Gln240, Ser242, Leu243, Leu244
PEN2	Leu3, Phe28, Leu31	Leu3, Phe28, Leu29, Leu31
C83	Gly13, Ala14, Lys37	Ala13, Gln14, His16, Arg39

Table S3. Intermolecular contact analysis for top clusters of γ-Secretase-C83 complexes (A: Nicastrin, B: PS1, and E: C83).

Simulation 1			Simulation 2			Simulation 3		
Interacting Pairs	**Distance**	**Category**	**Interacting Pairs**	**Distance**	**Category**	**Interacting Pairs**	**Distance**	**Category**
E:LEU688:HT3 - A:GLU650:OE1	1.70	Hydrogen Bond; Electrostatic	E:LEU688:HT3 - A:GLU650:OE1	1.50	Hydrogen Bond; Electrostatic	A:ASN34:HT3 - B:ASP403:OD2	3.18	Hydrogen Bond; Electrostatic
E:LYS725:HZ2 - B:GLU277:OE2	1.71	Hydrogen Bond; Electrostatic	E:LYS726:HZ1 - B:GLU376:OE1	1.64	Hydrogen Bond; Electrostatic	B:ARG108:HH21 - E:GLU693:OE2	3.03	Hydrogen Bond; Electrostatic
A:ASN34:N - B:ASP403:OD1	4.34	Electrostatic	E:LYS726:HZ2 - B:GLU280:OE2	1.83	Hydrogen Bond; Electrostatic	E:LEU688:HT3 - A:GLU650:OE1	1.83	Hydrogen Bond; Electrostatic
B:LYS187:NZ - A:GLU245:OE1	5.02	Electrostatic	B:ARG108:NH2 - E:GLU693:OE1	5.00	Electrostatic	E:LYS725:HZ1 - B:GLU280:OE1	2.62	Hydrogen Bond; Electrostatic
E:LEU688:N - A:ASP249:OD1	5.21	Electrostatic	B:LYS187:NZ - A:GLU245:OE1	5.16	Electrostatic	E:LYS725:HZ2 - B:GLU376:OE1	1.65	Hydrogen Bond; Electrostatic
A:ARG652:HH11 - E:VAL689:O	1.81	Hydrogen Bond	B:LYS239:NZ - E:GLU693:OE1	4.63	Electrostatic	E:LYS725:HZ3 - B:GLU280:OE2	1.89	Hydrogen Bond; Electrostatic
A:TRP653:HN - E:LEU688:O	2.01	Hydrogen Bond	E:LEU688:N - A:ASP249:OD2	5.27	Electrostatic	B:ARG108:NH1 - A:GLU245:OE2	5.06	Electrostatic
B:LYS380:HN - E:LEU723:O	2.09	Hydrogen Bond	A:ASN34:HD21 - B:ASP403:OD1	1.97	Hydrogen Bond	B:LYS187:NZ - A:GLU245:OE2	4.78	Electrostatic
B:GLY382:HN - E:VAL721:O	1.94	Hydrogen Bond	A:ASN243:HD22 - E:GLU693:OE1	2.09	Hydrogen Bond	B:LYS239:NZ - E:GLU693:OE2	4.71	Electrostatic
B:LEU432:HN - E:MET722:O	2.11	Hydrogen Bond	A:ILE246:HN - E:PHE691:O	2.66	Hydrogen Bond	E:LEU688:N - A:ASP249:OD2	5.09	Electrostatic
E:LEU688:HT2 - A:SER651:O	2.40	Hydrogen Bond	A:ARG652:HH11 - E:VAL689:O	1.81	Hydrogen Bond	A:ASN243:HD22 - E:LYS699:O	2.12	Hydrogen Bond
E:PHE690:HN - A:TRP653:O	2.14	Hydrogen Bond	A:TRP653:HN - E:LEU688:O	2.00	Hydrogen Bond	A:ARG652:HH11 - E:VAL689:O	1.92	Hydrogen Bond
E:LYS699:HZ2 - B:ASP110:O	1.82	Hydrogen Bond	B:GLN112:HN - E:ALA692:O	1.98	Hydrogen Bond	A:TRP653:HN - E:LEU688:O	2.31	Hydrogen Bond
E:LYS699:HZ3 - B:GLN112:O	1.71	Hydrogen Bond	B:TRP165:HE1 - E:ILE712:O	1.97	Hydrogen Bond	B:TRP165:HE1 - E:ILE712:O	1.95	Hydrogen Bond
E:ALA701:HN - A:ASN243:OD1	1.96	Hydrogen Bond	B:LYS380:HN - E:LEU723:O	2.79	Hydrogen Bond	B:LYS380:HN - E:LEU723:O	2.07	Hydrogen Bond
E:LEU720:HN - B:ASP257:OD2	1.92	Hydrogen Bond	B:LEU383:HN - E:THR719:OG1	2.23	Hydrogen Bond	B:GLY382:HN - E:VAL721:O	1.99	Hydrogen Bond

E:VAL721:HN - B:ASP385:OD2	1.74	Hydrogen Bond	B:GLY384:HN - E:THR719:OG1	2.56	Hydrogen Bond	B:LEU432:HN - E:MET722:O	2.26	Hydrogen Bond
E:MET722:HN - B:LEU432:O	2.14	Hydrogen Bond	E:LEU688:HT2 - A:SER651:O	2.17	Hydrogen Bond	E:LEU688:HT2 - A:SER651:O	2.05	Hydrogen Bond
E:LEU723:HN - B:LYS380:O	1.92	Hydrogen Bond	E:GLU693:HN - A:PRO244:O	1.82	Hydrogen Bond	E:PHE690:HN - A:TRP653:O	1.71	Hydrogen Bond
A:ARG652:HA - E:LEU688:O	2.38	Hydrogen Bond	E:LYS699:HZ1 - B:THR116:O	2.59	Hydrogen Bond	E:LEU720:HN - B:ASP257:OD2	1.86	Hydrogen Bond
A:ARG652:HD1 - E:LEU688:O	2.52	Hydrogen Bond	E:LYS699:HZ2 - B:TYR115:O	2.39	Hydrogen Bond	E:VAL721:HN - B:ASP385:OD1	2.01	Hydrogen Bond
A:ARG652:HD2 - E:VAL689:O	3.07	Hydrogen Bond	E:LYS699:HZ2 - B:PRO117:O	2.03	Hydrogen Bond	E:MET722:HN - B:LEU432:O	1.82	Hydrogen Bond
B:VAL379:HA - E:LEU723:O	2.84	Hydrogen Bond	E:LYS699:HZ3 - B:LEU113:O	1.79	Hydrogen Bond	E:LEU723:HN - B:LYS380:O	2.37	Hydrogen Bond
B:GLY382:HA1 - E:VAL721:O	3.03	Hydrogen Bond	E:LEU723:HN - B:LYS380:O	2.62	Hydrogen Bond	E:LYS725:HN - B:GLY378:O	2.09	Hydrogen Bond
B:ALA431:HA - E:MET722:O	2.78	Hydrogen Bond	A:ARG652:HA - E:LEU688:O	2.42	Hydrogen Bond	A:ARG652:HA - E:LEU688:O	2.34	Hydrogen Bond
E:VAL689:HA - A:TRP653:O	2.61	Hydrogen Bond	A:ARG652:HD1 - E:LEU688:O	2.55	Hydrogen Bond	A:ARG652:HD1 - E:LEU688:O	2.59	Hydrogen Bond
E:LYS699:HE1 - B:GLN112:O	2.63	Hydrogen Bond	A:ARG652:HD1 - E:VAL689:O	2.75	Hydrogen Bond	A:ARG652:HD2 - E:VAL689:O	2.61	Hydrogen Bond
E:THR719:HA - B:ASP257:OD2	2.71	Hydrogen Bond	A:ARG652:HD2 - E:VAL689:O	2.45	Hydrogen Bond	B:GLY111:HA1 - E:GLU693:OE1	2.69	Hydrogen Bond
E:LEU720:HA - B:ASP385:OD2	2.62	Hydrogen Bond	B:GLY382:HA1 - E:THR719:O	2.62	Hydrogen Bond	B:GLY111:HA2 - E:GLU693:OE1	2.40	Hydrogen Bond
E:MET722:HA - B:LYS380:O	2.79	Hydrogen Bond	B:GLY384:HA1 - E:VAL717:O	2.61	Hydrogen Bond	B:VAL379:HA - E:LEU723:O	2.32	Hydrogen Bond
E:LYS724:HE1 - B:TYR77:OH	2.91	Hydrogen Bond	E:PHE690:HA - A:TRP653:O	3.05	Hydrogen Bond	B:ALA431:HA - E:MET722:O	2.77	Hydrogen Bond
E:LYS724:HE2 - B:TYR77:OH	2.57	Hydrogen Bond	E:ALA692:HA - A:PRO244:O	2.88	Hydrogen Bond	E:ALA713:HA - B:SER169:OG	2.67	Hydrogen Bond
E:LYS724:HE2 - B:ARG377:O	2.38	Hydrogen Bond	E:LYS699:HE1 - B:PRO117:O	3.05	Hydrogen Bond	E:THR719:HA - B:ASP257:OD2	2.34	Hydrogen Bond
E:LEU688:N - A:TRP653	3.31	Electrostatic	E:LYS699:HE2 - B:LEU113:O	2.68	Hydrogen Bond	E:LEU720:HA - B:ASP385:OD1	2.57	Hydrogen Bond
E:MET706:SD - B:TYR240	5.57	Other	E:ALA713:HA - B:SER169:OG	2.28	Hydrogen Bond	E:VAL721:HA - B:LEU432:O	2.52	Hydrogen Bond

E:LEU688:C,O;VAL689:N - A:TRP653	4.00	Hydrophobic	E:LYS724:HE2 - B:GLN276:OE1	2.66	Hydrogen Bond	E:MET722:HA - B:LYS380:O	2.93	Hydrogen Bond
B:LEU85 - E:MET722	5.31	Hydrophobic	E:LYS726:HE2 - B:GLU280:OE1	2.92	Hydrogen Bond	E:LYS724:HA - B:GLY378:O	2.56	Hydrogen Bond
B:ILE114 - E:ILE703	4.61	Hydrophobic	E:LEU688:N - A:TRP653	3.24	Electrostatic	E:LEU688:N - A:TRP653	3.72	Electrostatic
B:VAL142 - E:VAL711	5.27	Hydrophobic	E:MET706:SD - B:PHE177	5.11	Other	E:VAL715:HB - B:TRP165	2.69	Hydrophobic
B:LEU173 - E:ILE712	5.07	Hydrophobic	E:LEU688:C,O;VAL689:N - A:TRP653	3.53	Hydrophobic	E:MET706:SD - B:PHE177	4.49	Other
B:VAL236 - E:MET706	5.17	Hydrophobic	E:LEU688:C,O;VAL689:N - A:TRP653	3.70	Hydrophobic	E:LEU688:C,O;VAL689:N - A:TRP653	3.61	Hydrophobic
B:VAL236 - E:VAL710	5.08	Hydrophobic	A:ILE242 - B:ILE180	4.51	Hydrophobic	E:LEU688:C,O;VAL689:N - A:TRP653	3.33	Hydrophobic
B:LEU286 - E:ILE716	5.50	Hydrophobic	A:VAL557 - E:LEU688	4.64	Hydrophobic	A:VAL557 - E:LEU688	4.65	Hydrophobic
B:VAL379 - E:MET722	5.39	Hydrophobic	B:ILE114 - E:ILE703	5.02	Hydrophobic	B:LEU150 - E:ILE718	4.97	Hydrophobic
B:LYS380 - E:LEU723	4.62	Hydrophobic	B:VAL142 - E:VAL711	4.84	Hydrophobic	B:ILE180 - E:ILE702	5.45	Hydrophobic
B:LEU381 - E:MET722	4.69	Hydrophobic	B:VAL236 - E:VAL710	5.45	Hydrophobic	B:ILE180 - E:MET706	4.96	Hydrophobic
B:LEU425 - E:MET722	4.80	Hydrophobic	B:VAL272 - E:VAL721	5.02	Hydrophobic	B:LEU282 - E:LEU723	4.93	Hydrophobic
B:ALA431 - E:VAL721	5.11	Hydrophobic	B:LEU286 - E:ILE716	4.60	Hydrophobic	B:VAL379 - E:MET722	5.32	Hydrophobic
B:ALA431 - E:LEU723	4.45	Hydrophobic	B:VAL379 - E:MET722	4.83	Hydrophobic	B:VAL379 - E:LYS724	4.97	Hydrophobic
B:ALA434 - E:MET722	4.49	Hydrophobic	B:LYS380 - E:LEU723	4.85	Hydrophobic	B:LYS380 - E:LYS725	4.88	Hydrophobic
B:LEU435 - E:LEU720	5.30	Hydrophobic	E:VAL710 - B:MET233	5.45	Hydrophobic	B:LEU381 - E:MET722	4.98	Hydrophobic
B:PRO436 - E:LEU720	5.26	Hydrophobic	E:ALA713 - B:MET233	4.95	Hydrophobic	B:LEU383 - E:ILE716	5.15	Hydrophobic
E:LYS699 - B:ILE114	4.43	Hydrophobic	E:VAL715 - B:LEU166	4.48	Hydrophobic	B:LEU425 - E:MET722	5.00	Hydrophobic
E:ALA701 - A:PRO244	5.39	Hydrophobic	A:TRP653 - E:VAL689	5.28	Hydrophobic	B:ALA431 - E:VAL721	5.49	Hydrophobic

E:ALA713 - B:LEU173	4.60	Hydrophobic	B:PHE105 - A:ILE242	4.89	Hydrophobic	B:ALA431 - E:LEU723	4.83	Hydrophobic
E:VAL715 - B:LEU166	5.27	Hydrophobic	B:TRP165 - E:VAL715	4.33	Hydrophobic	B:ALA434 - E:MET722	3.72	Hydrophobic
A:TRP653 - E:VAL689	5.40	Hydrophobic	B:TRP165 - E:VAL715	4.05	Hydrophobic	B:LEU435 - E:LEU720	5.06	Hydrophobic
B:HIS81 - E:LYS724	5.18	Hydrophobic	B:PHE237 - E:VAL710	5.07	Hydrophobic	E:ALA701 - A:ILE242	5.50	Hydrophobic
B:TRP165 - E:VAL715	4.63	Hydrophobic	B:PHE388 - E:VAL717	5.33	Hydrophobic	E:VAL707 - B:ILE114	4.68	Hydrophobic
B:PHE176 - E:LEU705	5.35	Hydrophobic	E:PHE690 - A:LYS654	4.25	Hydrophobic	E:ALA713 - B:MET233	5.13	Hydrophobic
B:PHE176 - E:MET706	5.30	Hydrophobic	E:PHE691 - A:ILE246	5.48	Hydrophobic	E:VAL721 - B:LEU268	4.95	Hydrophobic
B:PHE237 - E:VAL710	5.05	Hydrophobic				E:VAL721 - B:LEU282	4.99	Hydrophobic
B:PHE388 - E:VAL717	4.83	Hydrophobic				A:TRP653 - E:VAL689	4.95	Hydrophobic
E:PHE690 - A:LYS654	4.00	Hydrophobic				B:TRP165 - E:VAL715	4.15	Hydrophobic
E:PHE691 - A:ILE246	5.25	Hydrophobic				B:PHE176 - E:LEU705	5.28	Hydrophobic
						B:PHE176 - E:MET706	5.32	Hydrophobic
						B:PHE237 - E:VAL710	5.35	Hydrophobic
						B:TYR240 - E:MET706	5.44	Hydrophobic

Table S4. Intermolecular contact analysis of the top ranked clusters of γ-Secretase-Notch100 complexes (A: Nicastrin, B: PS1 and E: Notch100).

Simulation 1			Simulation 2			Simulation 3		
Interacting Pairs	**Distance**	**Category**	**Interacting Pairs**	**Distance**	**Category**	**Interacting Pairs**	**Distance**	**Category**
A:LYS654:HZ1 - E:GLU1727:OE2	2.81	Hydrogen Bond; Electrostatic	A:ARG652:HH12 - E:GLU1727:OE2	1.70	Hydrogen Bond; Electrostatic	B:ARG108:HH12 - A:GLU245:OE2	1.82	Hydrogen Bond; Electrostatic
A:LYS654:HZ2 - E:GLU1727:OE1	1.72	Hydrogen Bond; Electrostatic	A:ARG652:HH22 - E:GLU1727:OE1	2.01	Hydrogen Bond; Electrostatic	E:VAL1721:HT1 - A:ASP253:OD1	1.63	Hydrogen Bond; Electrostatic
B:LYS187:HZ2 - A:GLU245:OE2	1.67	Hydrogen Bond; Electrostatic	A:LYS654:HZ2 - E:GLU1724:OE2	1.65	Hydrogen Bond; Electrostatic	E:ARG1761:HH12 - B:GLU376:OE2	1.84	Hydrogen Bond; Electrostatic
B:ARG377:HH21 - E:ARG1761:OT1	2.01	Hydrogen Bond; Electrostatic	B:LYS187:HZ1 - A:GLU245:OE1	2.51	Hydrogen Bond; Electrostatic	E:ARG1761:HH22 - B:GLU376:OE2	1.78	Hydrogen Bond; Electrostatic
A:ASN34:N - B:ASP403:OD2	5.05	Electrostatic	E:VAL1721:HT3 - B:GLU120:OE1	1.64	Hydrogen Bond; Electrostatic	A:ARG38:NH2 - B:ASP458:OD2	5.45	Electrostatic
A:ARG652:NH1 - E:GLU1727:OE1	4.70	Electrostatic	E:ARG1760:HH12 - B:GLU273:OE1	2.17	Hydrogen Bond; Electrostatic	A:ARG629:NH1 - E:GLU1727:OE1	5.07	Electrostatic
A:ARG652:NH2 - E:GLU1724:OE2	5.16	Electrostatic	E:ARG1760:HH22 - B:GLU273:OE1	1.79	Hydrogen Bond; Electrostatic	B:ARG108:NH2 - A:GLU245:OE1	4.87	Electrostatic
B:ARG377:NH2 - E:ARG1761:OT2	5.04	Electrostatic	B:ARG108:NH1 - A:GLU245:OE2	5.19	Electrostatic	E:ARG1761:NH1 - B:GLU376:OE1	4.79	Electrostatic
A:ASN34:HD21 - B:SER401:O	2.65	Hydrogen Bond	E:ARG1760:NH1 - B:GLU273:OE2	4.76	Electrostatic	A:SER35:HG1 - B:ASP458:O	2.99	Hydrogen Bond
A:ASN34:HD22 - B:GLY402:O	2.88	Hydrogen Bond	A:ASN34:HD21 - B:ASP403:OD2	2.79	Hydrogen Bond	A:SER35:HG1 - B:ASP458:OD2	1.75	Hydrogen Bond
A:ASN243:HD21 - B:GLU184:OE1	1.70	Hydrogen Bond	A:ASN243:HD21 - B:GLU184:OE2	1.75	Hydrogen Bond	A:ASN243:HD21 - B:GLN112:OE1	2.93	Hydrogen Bond
A:ILE246:HN - E:GLU1727:O	2.09	Hydrogen Bond	B:GLY111:HN - E:THR1725:OG1	1.97	Hydrogen Bond	A:ASN243:HD22 - E:PRO1729:O	1.98	Hydrogen Bond
B:GLN112:HE22 - E:PRO1729:O	2.91	Hydrogen Bond	B:TYR195:HH - A:PHE240:O	1.98	Hydrogen Bond	A:ARG629:HH12 - E:GLN1722:O	1.96	Hydrogen Bond

B:GLN276:HE22 - E:ARG1758:O	2.75	Hydrogen Bond	B:GLN276:HE21 - E:ARG1758:O	2.66	Hydrogen Bond	A:ARG629:HH21 - E:GLN1722:O	2.37	Hydrogen Bond
B:LYS380:HN - E:SER1757:O	1.94	Hydrogen Bond	B:LYS380:HN - E:SER1757:O	1.98	Hydrogen Bond	B:LYS380:HN - E:SER1757:O	2.07	Hydrogen Bond
B:GLY382:HN - E:LEU1755:O	1.72	Hydrogen Bond	B:GLY382:HN - E:LEU1755:O	2.03	Hydrogen Bond	B:GLY382:HN - E:LEU1755:O	2.24	Hydrogen Bond
B:LEU383:HN - E:GLY1753:O	2.95	Hydrogen Bond	B:LEU383:HN - E:GLY1753:O	3.07	Hydrogen Bond	B:GLY384:HN - E:GLY1753:O	2.21	Hydrogen Bond
B:GLY384:HN - E:GLY1753:O	1.77	Hydrogen Bond	B:GLY384:HN - E:GLY1753:O	2.22	Hydrogen Bond	B:LEU432:HN - E:LEU1756:O	2.70	Hydrogen Bond
E:SER1723:HG1 - A:VAL557:O	1.78	Hydrogen Bond	B:LEU432:HN - E:LEU1756:O	2.70	Hydrogen Bond	E:VAL1721:HT3 - A:SER559:OG	1.77	Hydrogen Bond
E:LEU1755:HN - B:ASP385:OD1	2.04	Hydrogen Bond	E:GLN1722:HE21 - B:THR119:O	2.05	Hydrogen Bond	E:GLN1722:HE21 - A:SER559:O	1.96	Hydrogen Bond
E:SER1757:HN - B:LYS380:O	2.07	Hydrogen Bond	E:SER1723:HN - B:THR119:OG1	2.88	Hydrogen Bond	E:CYS1752:HG1 - B:THR147:OG1	1.93	Hydrogen Bond
E:ARG1758:HH22 - B:LYS429:O	3.02	Hydrogen Bond	E:SER1723:HG1 - B:LYS109:O	2.47	Hydrogen Bond	E:LEU1755:HN - B:ASP385:OD1	1.94	Hydrogen Bond
E:ARG1760:HN - B:GLN276:OE1	2.12	Hydrogen Bond	E:LEU1755:HN - B:ASP385:OD1	2.17	Hydrogen Bond	E:SER1757:HN - B:LYS380:O	2.48	Hydrogen Bond
E:ARG1761:HH11 - B:HIS81:NE2	2.57	Hydrogen Bond	E:SER1757:HN - B:LYS380:O	2.25	Hydrogen Bond	E:LYS1759:HN - B:GLY378:O	1.90	Hydrogen Bond
A:SER241:HA - B:TYR195:OH	2.89	Hydrogen Bond	E:ARG1758:HE - B:LYS429:O	2.99	Hydrogen Bond	E:LYS1759:HZ1 - B:MET292:O	3.09	Hydrogen Bond
A:GLU245:HA - E:GLU1727:O	2.30	Hydrogen Bond	E:LYS1759:HN - B:GLY378:O	2.54	Hydrogen Bond	E:LYS1759:HZ2 - B:MET292:O	2.63	Hydrogen Bond
B:ARG377:HD1 - E:ARG1760:O	2.32	Hydrogen Bond	E:LYS1759:HZ1 - B:GLN276:O	2.73	Hydrogen Bond	B:VAL379:HA - E:SER1757:O	2.94	Hydrogen Bond
B:ARG377:HD2 - E:ARG1761:OT1	2.78	Hydrogen Bond	E:ARG1760:HN - B:GLN276:OE1	1.75	Hydrogen Bond	B:GLY382:HA1 - E:GLY1753:O	2.60	Hydrogen Bond
B:VAL379:HA - E:SER1757:O	2.65	Hydrogen Bond	B:ASP110:HA - E:THR1725:OG1	2.73	Hydrogen Bond	B:GLY384:HA1 - E:VAL1750:O	2.93	Hydrogen Bond
B:GLY382:HA1 - E:GLY1753:O	2.99	Hydrogen Bond	B:THR119:HB - E:VAL1721:O	2.71	Hydrogen Bond	B:PHE462:HA - A:SER35:O	2.48	Hydrogen Bond
B:GLY382:HA1 - E:LEU1755:O	2.84	Hydrogen Bond	B:LYS187:HE1 - A:GLU245:OE1	3.10	Hydrogen Bond	E:VAL1754:HA - B:ASP385:OD1	2.49	Hydrogen Bond

E:PRO1728:HA - A:PRO244:O	2.59	Hydrogen Bond	B:VAL379:HA - E:SER1757:O	2.69	Hydrogen Bond	E:ARG1758:HA - B:GLY378:O	2.76	Hydrogen Bond
E:PRO1731:HD2 - B:GLN112:O	2.82	Hydrogen Bond	B:LEU381:HA - E:LEU1755:O	2.78	Hydrogen Bond	E:ARG1758:HD2 - B:ARG377:O	2.48	Hydrogen Bond
E:VAL1754:HA - B:ASP385:OD1	2.79	Hydrogen Bond	B:GLY382:HA1 - E:GLY1753:O	2.64	Hydrogen Bond	E:LYS1759:HE1 - B:SER289:OG	2.66	Hydrogen Bond
E:SER1757:HB1 - B:LYS380:O	2.53	Hydrogen Bond	B:ALA431:HA - E:LEU1756:O	2.85	Hydrogen Bond	A:ARG38:NH2 - B:PHE462	3.61	Electrostatic
E:LYS1759:HA - B:GLN276:OE1	2.81	Hydrogen Bond	E:SER1723:HB2 - B:LYS109:O	2.47	Hydrogen Bond	B:MET146:SD - E:PHE1744	5.49	Other
E:TYR1738:HH - B:PHE176	2.45	Hydrogen Bond	E:VAL1754:HA - B:ASP385:OD1	2.68	Hydrogen Bond	B:MET233:SD - E:PHE1749	5.71	Other
B:MET146:SD - E:PHE1748	5.29	Other	E:LEU1756:HA - B:LYS380:O	2.76	Hydrogen Bond	B:PHE176 - E:TYR1738	5.18	Hydrophobic
B:TRP165 - E:PHE1748	5.03	Hydrophobic	E:ARG1758:HA - B:GLY378:O	2.60	Hydrogen Bond	A:ILE242 - B:LEU113	5.38	Hydrophobic
B:PHE176 - E:TYR1738	5.10	Hydrophobic	E:LYS1759:HA - B:GLN276:OE1	2.66	Hydrogen Bond	A:ARG629 - E:VAL1721	5.14	Hydrophobic
A:ILE242 - B:ILE180	4.69	Hydrophobic	E:TYR1738:HH - B:PHE176	2.29	Hydrogen Bond	B:MET139 - E:LEU1747	5.16	Hydrophobic
A:PRO244 - E:PRO1729	5.14	Hydrophobic	B:MET146:SD - E:PHE1748	3.58	Other	B:LEU172 - E:LEU1746	5.34	Hydrophobic
B:VAL142 - E:LEU1747	5.23	Hydrophobic	B:PHE176 - E:TYR1738	5.17	Hydrophobic	B:LEU173 - E:LEU1746	4.98	Hydrophobic
B:LEU173 - E:LEU1746	4.93	Hydrophobic	B:MET139 - E:LEU1747	4.83	Hydrophobic	B:MET233 - E:LEU1746	4.62	Hydrophobic
B:MET233 - E:LEU1746	4.67	Hydrophobic	B:VAL142 - E:LEU1747	4.67	Hydrophobic	B:VAL236 - E:LEU1746	5.47	Hydrophobic
B:LEU268 - E:LEU1755	4.76	Hydrophobic	B:MET233 - E:LEU1746	5.32	Hydrophobic	B:VAL261 - E:LEU1755	5.40	Hydrophobic
B:ARG377 - E:LYS1759	4.22	Hydrophobic	B:ARG377 - E:LYS1759	4.57	Hydrophobic	B:LEU268 - E:LEU1755	4.64	Hydrophobic
B:ARG377 - E:ARG1761	4.83	Hydrophobic	B:LEU425 - E:LEU1756	4.32	Hydrophobic	B:VAL272 - E:LEU1755	5.05	Hydrophobic
B:LEU425 - E:LEU1756	4.73	Hydrophobic	B:ALA434 - E:LEU1756	4.13	Hydrophobic	B:LYS380 - E:LYS1759	4.83	Hydrophobic
B:ALA434 - E:LEU1756	4.55	Hydrophobic	E:PRO1731 - B:LEU113	4.42	Hydrophobic	B:LEU381 - E:LEU1756	5.25	Hydrophobic
E:PRO1731 - B:LEU113	5.22	Hydrophobic	E:VAL1739 - B:LEU113	5.06	Hydrophobic	B:LEU425 - E:LEU1756	4.52	Hydrophobic

E:VAL1739 - B:LEU113	4.67	Hydrophobic	E:VAL1739 - B:ILE114	5.39	Hydrophobic	B:ALA434 - E:LEU1756	4.25	Hydrophobic
E:VAL1739 - B:ILE114	5.10	Hydrophobic	E:ALA1742 - B:LEU172	4.75	Hydrophobic	E:PRO1731 - A:ILE242	4.76	Hydrophobic
E:ALA1742 - B:LEU172	4.22	Hydrophobic	E:VAL1750 - B:MET233	4.95	Hydrophobic	E:PRO1731 - B:LEU113	4.39	Hydrophobic
E:ALA1743 - B:ILE114	5.02	Hydrophobic	E:VAL1750 - B:ILE387	5.07	Hydrophobic	E:VAL1739 - B:LEU113	5.22	Hydrophobic
E:VAL1745 - B:ILE168	5.05	Hydrophobic	E:CYS1752 - B:MET146	5.49	Hydrophobic	E:ALA1742 - B:LEU172	4.45	Hydrophobic
E:VAL1750 - B:ILE387	5.39	Hydrophobic	E:CYS1752 - B:LEU150	5.49	Hydrophobic	E:VAL1750 - B:MET233	4.94	Hydrophobic
E:CYS1752 - B:LEU150	4.38	Hydrophobic	E:VAL1754 - B:LEU435	5.09	Hydrophobic	E:VAL1750 - B:ILE387	4.93	Hydrophobic
E:CYS1752 - B:LEU268	5.16	Hydrophobic	E:ARG1758 - B:VAL379	4.55	Hydrophobic	E:CYS1752 - B:LEU150	4.98	Hydrophobic
E:VAL1754 - B:LEU435	5.41	Hydrophobic	E:ARG1758 - B:LEU425	4.75	Hydrophobic	E:ARG1758 - B:LEU425	5.25	Hydrophobic
E:ARG1758 - B:VAL379	5.16	Hydrophobic	E:ARG1760 - B:LYS430	4.60	Hydrophobic	A:TYR254 - E:VAL1721	5.40	Hydrophobic
E:ARG1758 - B:LEU425	4.85	Hydrophobic	B:PHE388 - E:VAL1750	5.02	Hydrophobic	B:PHE237 - E:VAL1750	5.03	Hydrophobic
B:TRP165 - E:VAL1745	5.29	Hydrophobic	E:PHE1748 - B:LEU166	5.20	Hydrophobic	B:PHE388 - E:VAL1750	4.90	Hydrophobic
B:PHE179 - A:ILE242	5.38	Hydrophobic				B:PHE462 - A:ARG38	5.00	Hydrophobic
B:PHE388 - E:VAL1750	5.41	Hydrophobic				B:PHE462 - A:LYS39	4.59	Hydrophobic

Table S5. MM/PBSA Binding Free Energy (kJ mol^{-1}) of γ-secretase with C83 and Notch100 complexes computed using 500 snapshots from the last 300 ns trajectory of both the complexes

Complex System	**Δ_{vdW}**	**Δ_{elec}**	**Δ_{ps}**	**Δ_{sasa}**	**ΔG_{Total}**
C83 (Simulation 1)	-867.16 ±1.50	-410.54 ± 7.30	1189.10 ± 8.41	-106.41 ± 0.17	-195.31 ± 2.82
C83 (Simulation 2)	-795.21 ±1.66	-806.18 ± 5.49	1512.07 ± 6.13	-107.64 ± 0.17	-196.94 ± 3.76
C83 (Simulation 3)	-904.86 ±1.77	-605.66 ± 4.71	1334.70 ± 5.31	-112.00 ± 0.15	-288.01 ± 2.83
Notch100 (Simulation 1)	-920.88 ± 1.91	-388.39 ± 7.79	984.68 ± 8.65	-115.25 ± 0.21	-251.16 ± 3.36
Notch100 (Simulation 2)	-873.96 ±1.64	-406.65 ± 6.55	998.03 ± 7.77	-109.84 ± 0.15	-184.20 ± 4.69
Notch100 (Simulation 3)	-898.27 ± 1.57	-440.79 ± 5.59	974.68 ± 6.39	-118.74 ± 0.18	-172.19 ± 3.65

* Δ_{vdW}: Van derWaals energy, Δ_{elec}: electrostatic energy, Δ_{ps}:polar solvation energy, Δ_{sasa}: solvent accessible surface area energy ΔG_{Tota}: total binding free energy

Table S6. Distribution of tilt angles of TMs in C83 and Notch100-γ-secretase complexes computed from the last 300 ns of each trajectory.

Systems	Simulations	Property	TM1	TM2	TM3	TM4	TM5	TM6	TM6a	TM7	TM8	TM9	TM (C83/ Notch100)
C83-Complex	Simulation 1	Average	10.94	11.76	6.97	6.41	5.93	8.44	17.21	6.53	6.85	8.57	10.43
		Std Dev	4.43	3.45	1.11	1.55	1.39	1.91	8.33	1.44	1.32	2.01	2.80
	Simulation 2	Average	11.53	6.93	7.07	6.50	8.11	6.24	10.27	6.02	10.75	8.94	9.27
		Std Dev	2.07	1.45	0.99	1.40	1.92	1.33	3.80	1.54	1.88	1.32	2.12
	Simulation 3	Average	7.47	6.80	10.12	7.63	9.07	13.22	49.48	7.18	8.19	11.01	7.20
		Std Dev	1.44	1.98	1.59	1.94	2.66	2.51	5.64	1.92	1.44	2.76	2.06
Notch100-Complex	Simulation 1	Average	7.25	8.52	6.31	5.74	5.10	8.09	7.93	7.85	8.05	8.05	5.88
		Std Dev	1.62	2.37	1.14	1.52	1.18	1.85	2.48	2.14	1.64	1.64	1.58
	Simulation 2	Average	6.14	6.59	6.38	6.09	7.11	5.87	7.94	7.42	5.62	7.99	7.98
		Std Dev	1.29	1.49	1.36	1.52	1.84	1.37	2.60	2.27	1.47	1.76	1.87
	Simulation 3	Average	6.47	8.82	6.75	7.79	5.73	8.30	12.41	6.65	7.18	6.89	6.61
		Std Dev	1.25	1.76	1.68	2.01	1.67	1.69	4.05	1.67	1.49	1.33	1.64

References

(1) Mehra, R.; Dehury, B.; Kepp, K. P. Cryo-Temperature Effects on Membrane Protein Structure and Dynamics. *Phys. Chem. Chem. Phys.* **2020**, *in press.*, 5427–5438.

(2) Somavarapu, A. K.; Kepp, K. P. Membrane Dynamics of γ-Secretase Provides a Molecular Basis for β-Amyloid Binding and Processing. *ACS Chem. Neurosci.* **2017**, *8* (11), 2424–2436. https://doi.org/10.1021/acschemneuro.7b00208.

(3) Dehury, B.; Tang, N.; Kepp, K. P. K. P. Molecular Dynamics of C99-Bound γ-Secretase Reveal Two Binding Modes with Distinct Compactness, Stability, and Active-Site Retention: Implications for Aβ Production. *Biochem. J.* **2019**, *476* (7), BCJ20190023. https://doi.org/10.1042/BCJ20190023.

(4) Karplus, M.; McCammon, J. A. Molecular Dynamics Simulations of Biomolecules. *Nat. Struct. Biol.* **2002**, *9* (9), 646–652. https://doi.org/10.1038/nsb0902-646.

(5) Zhou, R.; Yang, G.; Guo, X.; Zhou, Q.; Lei, J.; Shi, Y. Recognition of the Amyloid Precursor Protein by Human γ-Secretase. *Science (80-.).* **2019**, *363* (6428), eaaw0930. https://doi.org/10.1126/science.aaw0930.

(6) Yang, G.; Zhou, R.; Zhou, Q.; Guo, X.; Yan, C.; Ke, M.; Lei, J.; Shi, Y. Structural Basis of Notch Recognition by Human γ-Secretase. *Nature* **2019**, *565* (7738), 192–197. https://doi.org/10.1038/s41586-018-0813-8.

(7) Hitzenberger, M.; Zacharias, M. γ-Secretase Studied by Atomistic Molecular Dynamics Simulations: Global Dynamics, Enzyme Activation, Water Distribution and Lipid Binding. *Front. Chem.* **2019**, *6*, 640. https://doi.org/10.3389/fchem.2018.00640.

(8) Aguayo-Ortiz, R.; Chávez-García, C.; Straub, J. E.; Dominguez, L. Characterizing the Structural Ensemble of γ-Secretase Using a Multiscale Molecular Dynamics Approach. *Chem. Sci.* **2017**, *8* (8), 5576–5584. https://doi.org/10.1039/c7sc00980a.

(9) Bai, X. C.; Rajendra, E.; Yang, G.; Shi, Y.; Scheres, S. H. H. W. Sampling the Conformational Space of the Catalytic Subunit of Human G-Secretase. *Elife* **2015**, *4*, 551–560. https://doi.org/10.7554/eLife.11182.

(10) Dominguez, L.; Foster, L.; Straub, J. E.; Thirumalai, D. Impact of Membrane Lipid Composition on the Structure and Stability of the Transmembrane Domain of Amyloid Precursor Protein. *Proc. Natl. Acad. Sci.* **2016**. https://doi.org/10.1073/pnas.1606482113.

(11) Aguayo-Ortiz, R.; Dominguez, L. Simulating the γ-Secretase Enzyme: Recent Advances and Future Directions. *Biochimie* **2018**, *147*, 130–135. https://doi.org/10.1016/j.biochi.2018.01.007.